Chapter 11
Theoretical Study of Oxygen Reduction Reaction Catalysts: From Pt to Non-precious Metal Catalysts

Xin Chen, Dingguo Xia, Zheng Shi, and Jiujun Zhang

Abstract Fuel cells are regarded as one of the most promising candidates for stationary and mobile power generation due to their high energy yield and low environmental impact of hydrogen oxidation. The oxygen reduction reaction (ORR) at cathode is a very complex process and plays a crucial role during operation of the PEM fuel cells. However, its mechanism and the nature of intermediates involved remain vague. This chapter focuses on the recent theoretical modeling studies of ORR catalysts for PEMFC. Recent theoretical investigations on oxygen reduction electrocatalysts, such as Pt-based catalysts, non-Pt metal catalysts (Pd, Ir, CuCl), and non-precious metal catalysts (transitional metal macrocyclic complexes, conductive polymer materials, and carbon-based materials), are reviewed. The oxygen reduction mechanisms catalyzed by these catalysts are discussed based on the results.

X. Chen
College of Environmental and Energy Engineering, Beijing University of Technology, Xidawang Road, Chaoyang District, Beijing 100124, P. R. China

D. Xia (✉)
College of Engineering, Peking University, No.5 Yiheyuan Road, Haidian District, Beijing 100871, P. R. China
e-mail: dgxia@pku.edu.cn

Z. Shi
NRC-Institute for Fuel Cell Innovation, 4250 Wesbrook Mall, Vancouver, British Columbia, Canada

J. Zhang (✉)
NRC Energy, Mining & Environment Portfolio, National Research Council Canada, 4250 Wesbrook Mall, Vancouver, BC, CanadaV6T 1W5
e-mail: jiujun.zhang@nrc.gc.ca

M. Shao (ed.), *Electrocatalysis in Fuel Cells*, Lecture Notes in Energy 9,
DOI 10.1007/978-1-4471-4911-8_11,

11.1 Introduction

Fuel cells are electrochemical devices that directly convert the chemical energy of a fuel into electrical energy by electrochemical reactions. Since their invention in the middle of the nineteenth century, fuel cells have been identified as the most promising energy conversion technology and have been successfully used in many specific areas, including space exploration. Fuel cells offer many advantages such as high efficiency and reliability, minimum impact to environment, unique operating characteristics, and so on.

There exist a variety of fuel cells. For practical reasons, fuel cells are classified by the type of electrolyte employed. The following names and abbreviations are frequently used in publications: alkaline fuel cells (AFC), molten carbonate fuel cells (MCFC), phosphoric acid fuel cells (PAFC), solid oxide fuel cells (SOFC), and proton exchange membrane fuel cells (PEMFC). Among different types of fuel cells under development today, the PEMFC, also called polymer electrolyte membrane fuel cells (PEFC), is considered as a potential future power source due to its unique characteristics [1–3]. The PEMFC consists of an anode where hydrogen oxidation takes place, a cathode where oxygen reduction occurs, and an electrolyte membrane that permits the transfer of protons from anode to cathode. PEMFC operates at low temperature that allows rapid start-up. Furthermore, with the absence of corrosive cell constituents, the use of the exotic materials required in other fuel cell types is not required [4].

Although PEMFC has many advantages compared with other kinds of fuel cells, there are several barriers challenging PEMFC's commercialization. These barriers are performance, cost, and durability. PEMFCs are sensitive to poisoning by trace levels of contaminants including CO, sulfur species, and ammonia. The high overpotential from oxygen reduction at cathode contributes significantly to performance losses [5]. Under PEMFC's operating environment, platinum can react with water and oxygen forming a surface oxide layer that inhibits the catalysis of the oxygen reduction reaction (ORR) especially at high potential [6, 7]. Thus development of more efficient ORR electrocatalysts and reducing their cost are the major focuses for advancing PEMFC technology.

ORR is a very complex process. It involves multi-electrons, various intermediates, and many possible pathways [8–10]. Different experimental characterization methods have been employed to study the ORR mechanism, such as ultraviolet photoemission spectroscopy (UPS) [11], X-ray photoemission spectroscopy (XPS) [12, 13], electron energy loss spectroscopy (EELS) [14], near-edge X-ray absorption spectroscopy (NEXAFS), and Auger spectroscopy (AES) [15, 16]. Despite all these studies, the nature of intermediates involved in the reduction steps remains vague. First-principle theoretical modeling is a good tool complementing state-of-the-art experimental techniques [17]. It provides important insights regarding electronic structure, geometries of reaction intermediates, and adsorption energies at metal/gas or metal/liquid interfaces. Theoretical modeling is becoming an indispensible tool in electrochemical study [18].

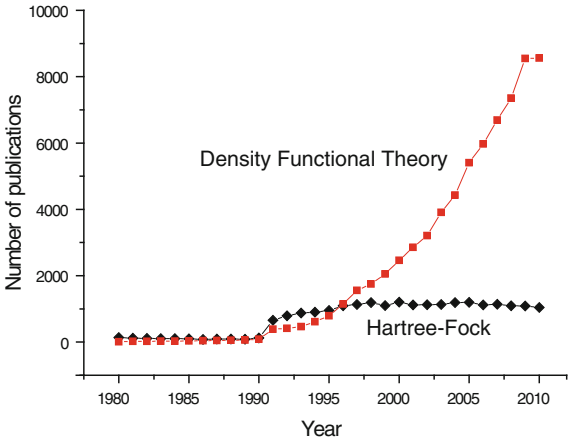

Fig. 11.1 Number of publications that employ DFT each year (from 1980 to September 23, 2011) based on search from Web of Science database (http://apps.webofknowledge.com) using "density," "functional," and "theory" as the keywords. This is compared with a similar search for keywords "Hartree" and "Fock," using Web of Science database

This chapter focuses on the theoretical modeling studies of ORR catalysts for PEMFC. Theoretical methods, such as density functional theory (DFT) and ab initio molecular dynamics (AIMD) simulation, are presented. Current understanding of ORR mechanism in acidic medium is briefly discussed. Recent theoretical investigations on oxygen reduction electrocatalysts, such as Pt-based catalysts, non-Pt metal catalysts (Pd, Ir, CuCl), and non-precious metal catalysts (transitional metal macrocyclic complexes, conductive polymer materials, and carbon-based materials), are reviewed. The oxygen reduction mechanisms catalyzed by these catalysts are discussed based on the results.

11.2 Computational Methods

11.2.1 Density Functional Theory Methods

DFT has become increasingly the method of choice for the solution of large systems, not only because of its sufficiently high accuracy but also of its computational simplicity. DFT reduces the calculation of system of many interacting particles to the solution of single-particle Hartree-type equations. Figure 11.1 shows the usage of DFT method from the year of 1980, as compared with the application of Hartree–Fock method.

In DFT, a many-electron (N) system is considered as a fictitious system of N noninteracting electrons which is described by a single determinant wave function with N "orbitals" φ_i. The electron density of this fictitious state can be obtained exactly by solving a set of one-electron Schrödinger equations (Kohn–Sham orbital) [19]. The Kohn–Sham self-consistent equation can be described as

$$\left[-\frac{1}{2}\nabla^2 + V_{\text{eff}}(r)\right]\varphi_i = \varepsilon_i\varphi_i \tag{11.1}$$

The effective external potential, $V_{\text{eff}}(r)$, is described as

$$V_{\text{eff}}(r) = V(r) + \int \frac{\rho(r')}{|r - r'|}\mathrm{d}r' + V_{\text{XC}}(r) \tag{11.2}$$

where $V(r)$ is the external potential, $\int \frac{\rho(r')}{|r-r'|}\mathrm{d}r'$ is Hartree potential, and $V_{\text{XC}}(r)$ is the exchange–correlation potential. The ground-state energy is given by

$$E = \sum_i^N \varepsilon_i - \frac{1}{2}\int\int \frac{\rho(r)\rho(r')}{|r - r'|}\mathrm{d}r\mathrm{d}r' + E_{\text{XC}}[\rho] - \int V_{\text{XC}}(r)\rho(r)\mathrm{d}r \tag{11.3}$$

In spite of the appearance of simplicity, the Kohn–Sham equation is in principle "exact" provided that the exact exchange–correlation energy E_{XC} is used. In other words, the only error in Eq. (11.3) is due to the approximate nature of E_{XC}.

Since the exact exchange–correlation term is unknown, several different schemes have been developed to obtain approximation of the E_{XC}. There are several types of approximate functionals such as local density approximation (LDA) and generalized gradient approximation (GGA) [20]. The LDA is very successful for many systems of interest, especially those with uniform electronic density distributions such as those in bulk metals, but LDA fails in systems where weak molecular bonds exist [21]. To account for the inhomogeneity of the electron density, a nonlocal correlation is often added to the exchange energy; this is the so-called generalized gradient approximation (GGA). There are several exchange–correlation functionals such as P86 [22], PW91 [23, 24], BPW91 [25], LYP [26], BLYP [20, 26], B3LYP [25–27], and PBE [28]. In general, as the exchange–correlation functional contains both exchange and Coulomb correlation terms, the DFT methods provide better results than that of a single determinant Hartree–Fock (HF) methods which do not have Coulomb correlation term [5].

The selection of functional directly controls the accuracy of the DFT methods. A study of ORR by hybrid density functional (HDFT) method and MP2 method has been reported by Albu et al. [29, 30]. They evaluated a large number of HDFT methods toward calculation of potential-dependent activation energies for uncatalyzed and Pt-catalyzed oxygen reduction and hydroperoxyl oxidation reactions. In the HDFT methods, the one-parameter hybrid Fock–Kohn–Sham operator is written as

$$F = F^{\text{H}} + \left(\frac{X}{100}\right)F^{\text{HFE}} + \left[1 - \left(\frac{X}{100}\right)\right](F^{\text{SE}} + F^{\text{GCE}}) + F^{\text{C}} \tag{11.4}$$

where F^{H} is the Hartree operator (i.e., the non-exchange part of the Hartree–Fock operator), F^{HFE} is the Hartree–Fock (HF) exchange operator, X is the fraction of Hartree–Fock exchange, F^{SE} is the Dirac–Slater local density functional for exchange, F^{GCE} is the gradient correction for the exchange functional, and F^{C} is the total correlation functional including both local and gradient-corrected parts.

Table 11.1 lists results obtained from MP2/6-31G(d,p) and various HDFT methods for uncatalyzed ORR. Table 11.2 contains results obtained with MP2/6-31G(d,p) and a subset of HDFT methods for Pt-catalyzed ORRs. In the tables, HDFT methods are named by the gradient-correlated exchanged functional used, followed by 1 (indicating a one-parameter method), followed by the correlation functional used, and finally by the value of X separated by a dash. For example, mPW1B95-50 represents a one-parameter hybrid DFT method based on the modified Perdew–Wang (mPW) gradient-corrected exchange functional [31] and B95 gradient-corrected correlation functional [32], and with a Hartree–Fock exchange contribution of 50 % ($X = 50$).

The results indicate that the inclusion of diffuse functions for oxygen by using the 6-31+G(d,p) basis set is unnecessary and gives inferior results. The HDFT methods with low HF exchange contributions show typically larger errors in comparison with the results obtained with the MP2 method. These errors are a consequence of a systematic underestimation of the transition-state energy for oxygen reduction to hydroperoxyl and hence its reverse hydroperoxyl oxidation reaction. Among the 25 HDFT methods investigated, the best results were obtained using the HDFT method based on Becke's exchange functional, B95 correlation functional, and a Hartree–Fock exchange contribution of 50 % in conjunction with the 6-31G(d,p) basis set [B1B95-50/6-31G(d,p)]. Results with similar accuracy were obtained using the HDFT method based on Becke's exchange functional, PW91 correlation functional, and a Hartree–Fock exchange contribution of 50 % in conjunction with the 6-31G(d,p) basis set [B1PW91-50/6-31G(d,p)]. Both of these methods also give very accurate gas-phase bond energies for the oxygenated species. Based on the calculated results, these two methods are recommended for study of electrochemical ORR.

11.2.2 Ab Initio Molecular Dynamics Method

Recently, ab initio or the first-principle molecular dynamics (AIMD), which is based on Car and Parrinello's technique [33], has become a valuable method for study condensed matter structure and dynamics, in particular liquids, surfaces, and clusters. The basic idea underlying AIMD method is to compute the forces acting on the nuclei from electronic structure that are calculated "on the fly" as the molecular dynamics trajectory is generated [34]. In this way, the electronic variables are not integrated out beforehand, but are considered as active degrees of freedom. Thus, the Car and Parrinello (CP) algorithm overcomes limitations of standard empirical-potential approaches employed in classical molecular dynamics and

Table 11.1 Comparison of calculated reversible potential for $O_2 + 4H^+ + 4e^- \rightarrow 2H_2O$ reaction, electrochemical potentials (V) and activation energies (eV) for $O_2 + H_3O^+ + e^- \rightarrow OOH + H_2O$ reaction, and the average relative error to the MP2/6-31G(d,p) results [29]

Basis set/HDFT method	X^a	$U°$(V)	$(U)E_a^{red} = 0$	$(E_a^{oxi})U_{red} = 0$	$(U)E_a^{oxi} = 0$	$(E_a^{red})U_{oxi} = 0$	Error
MP2/6-31G(d,p)		1.12	−1.867	2.278	3.513	3.102	0.00
6-31G(d,p)							
B3PW91	20	1.12	−0.998	1.907	3.221	2.312	0.89
B3LYP	20	1.20	−0.837	1.816	3.301	2.322	0.97
BH&HLYP	50	1.24	−1.293	2.233	3.865	2.925	0.48
PBE1PBE	25	1.03	−1.084	1.910	3.213	2.387	0.82
mPW1PW91	25	1.10	−1.069	1.958	3.296	2.406	0.80
MPW1K	42.8	1.22	−1.240	2.193	3.708	2.755	0.52
mPW1PW91-60	60	1.32	−1.318	2.345	4.010	2.983	0.53
B1B95	28	1.06	−1.225	1.984	3.211	2.452	0.71
BB1K	42	1.17	−1.395	2.216	3.614	2.793	0.40
B1B95-50	50	1.22	−1.436	2.289	3.778	2.924	0.38
B1B95-60	60	1.28	−1.464	2.363	3.950	3.051	0.43
mPW1B95	31	1.08	−1.233	2.023	3.345	2.554	0.63
MPWB1K	44	1.16	−1.351	2.188	3.643	2.806	0.42
mPW1B95-50	50	1.20	−1.387	2.247	3.764	2.904	0.40
6-31G+(d,p)							
B3PW91	20	1.92	−0.448	1.913	3.787	2.323	1.15
B3LYP	20	2.08	−0.207	1.828	3.952	2.331	1.30
BH&HLYP	50	2.00	−0.695	2.178	4.361	2.878	1.03
PBE1PBE	25	1.83	−0.500	1.891	3.783	2.392	1.09
mPW1PW91	25	1.89	−0.506	1.948	3.852	2.410	1.09
MPW1K	42.8	1.91	−0.715	2.152	4.166	2.729	0.96
mPW1PW91-60	60	1.94	−0.833	2.283	4.377	2.927	0.96
B1B95	28	1.87	−0.650	1.981	3.791	2.461	0.98
BB1K	42	1.90	−0.845	2.178	4.111	2.778	0.85
mPW1B95	31	1.89	−0.637	2.002	3.920	2.555	0.97
MPWB1K	44	1.90	−0.782	2.144	4.147	2.786	0.90

[a]Hartree–Fock exchange contribution X

Table 11.2 Electrochemical potentials and activation energies (eV) for Pt–O_2 + H_3O^+ + e^- → Pt–OOH + H_2O reaction and the average relative error to the MP2/6-31G(d,p) results [29]

HDFT method	$(U)E_a^{red} = 0$	$(E_a^{oxi})U_{red} = 0$	$(U)E_a^{oxi} = 0$	$(E_a^{red})U_{oxi} = 0$	Error
MP2/6-31G(d,p)[a]	0.382	1.330	2.681	0.969	0.00
B3PW91/6-31G(d,p)	0.929	0.529	2.280	0.822	0.70
BH&HLYP/6-31G(d,p)	0.493	0.846	2.651	1.312	0.42
MPW1K/6-31G(d,p)	0.633	0.762	2.651	1.256	0.45
mPW1PW91-60/6-31G(d,p)	0.470	0.904	2.709	1.335	0.40
B1B95-50/6-31G(d,p)	0.451	0.877	2.636	1.307	0.40
mPW1B95-50/6-31G(d,p)	0.475	0.862	2.661	1.324	0.42

The electrochemical potentials are in V, and the activation energies are in eV
[a]The basis set used for platinum is LANL2DZ

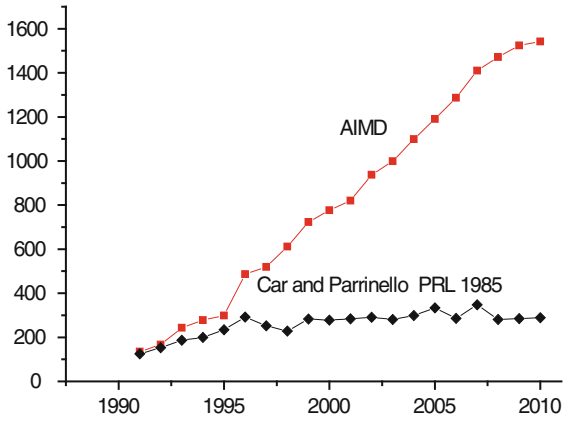

Fig. 11.2 Publication and citation analysis. *Squares*: number of publications with usage of AIMD each year from 1991 to September 28, 2011, which is based on Web of Science database (http://apps.webofknowledge.com) using "ab initio" and "molecular dynamics" (or synonym such as "first-principle MD" and "Car–Parrinello simulations") as the keywords. *Diamonds*: number of publications which cite the 1985 paper by Car and Parrinello [33]

provides direct information about the electronic structure. Figure 11.2 depictures the number of publications related to AIMD method.

The CP method makes use of the following classical Lagrangian

$$L_{CP} = \sum_i \frac{1}{2}\mu_i \langle \psi_i | \psi_i \rangle + \frac{1}{2}\sum_I M_I \dot{R}_I^2 - E(\psi_0, \vec{R}) + \text{constraints} \tag{11.5}$$

to generate trajectories for the nuclear and electronic degrees of freedom via the coupled set of equations of motion:

$$M_I \ddot{R}_I(t) = -\frac{\partial}{\partial R_I}\langle \psi_0 | H | \psi_0 \rangle + \frac{\partial}{\partial R_I}\{\text{constraints}\} \tag{11.6}$$

$$\mu_i \ddot{\psi}_i(t) = -\frac{\partial}{\partial \psi_i^*}\langle \psi_0 | H | \psi_0 \rangle + \frac{\partial}{\partial \psi_i^*}\{\text{constraints}\} \tag{11.7}$$

where $|\psi_0\rangle = \det\{\psi_i\}$ is the total wave function; M_I and R_I are atom I's nuclear mass and position, respectively; μ_i are the "fictitious electron masses" or inertia parameters assigned to the orbital degrees of freedom; and E is the energy functional of the system. For a given nuclear geometry, the ground-state electronic wave function can be obtained by standard techniques such as steepest descent or other higher order methods:

$$\dot{\psi}_i(t) = -\frac{1}{2}\frac{\delta E}{\delta \psi} + \sum_j \Lambda_{ij}\psi(t) = -\frac{1}{2}H\psi_i(t) + \sum_j \Lambda_{ij}\psi(t) \tag{11.8}$$

where Λ_{ij} are Lagrange multipliers which impose orthonormality constraints on the electronic orbitals. Thus, once the ground-state wave function has been determined, the dynamical behavior of a system can be studied at a given time; the force acting on the nuclei is given by Eq. (11.6). In the dynamical simulation, both the electronic and nuclear (ionic) degrees of freedom can propagate concurrently [35].

Compared to ordinary quantum chemical approaches, the AIMD free-energy calculations have significant advantage as entropic effects and anharmonicity are explicitly included in the calculation. In contrast, a normal static DFT procedure requires that the vibrational entropy be added via harmonic frequency calculations and the computational demands may be quite substantial for large molecular systems. Furthermore, the harmonic approximation may not even be valid in situations where weak interactions are dominant.

11.3 ORR in Acidic Medium

The ORR is a multi-electron reaction that includes a number of elementary reactions. Yeager proposed two pathways for the ORR in acidic medium [36]: (1) a "direct" four-electron pathway where O_2 is reduced directly to water without involvement of hydrogen peroxide (H_2O_2), $O_2 + 4H^+ + 4e^- \rightarrow 2H_2O$ and (2) a "series" pathway in which O_2 is reduced to H_2O_2, $O_2 + 2H^+ + 2e^- \rightarrow H_2O_2$, followed by its further reduction to H_2O, $H_2O_2 + 2H^+ + 2e^- \rightarrow 2H_2O$. Adzic et al. proposed a parallel pathway, with the direct and series mechanisms occur simultaneously, with the direct pathway as the dominant one [37].

For transition metal catalysts, two-electron reduction was reported for less active metals such as Au and Hg. For the most active catalyst, Pt and Pt-based alloys, four-electron reduction steps are generally believed. However, the detailed mechanism and reduction pathways are not clear and much debate remains. Even for the first electron transfer step, different views still exist [38–40]. Examples of plausible first steps include the following: (1) splitting of the O–O bond upon oxygen adsorption on two Pt sites (S) in a bridge configuration, $O_2 + 2S \rightarrow O^* + O^*$; (2) formation of

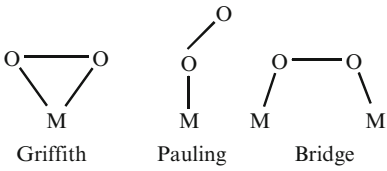

Fig. 11.3 Models of O_2 adsorption on electrode surfaces

the superoxide anion, $O_2 + 2S + e^- \rightarrow O_2^-$; and (3) simultaneous electron and proton transfer, $O_2 + 2S + (H^+ + e^-) \rightarrow OOH$.

O_2 reduction pathways were affected to a great extent by the O_2 adsorption modes on catalyst surfaces. There are three adsorption models for molecular oxygen adsorption (Fig. 11.3):

1. O_2 interacts with a single substrate atom (Griffith model) [41] forming a bond between its σ-orbitals and the empty d_{z^2} orbitals of the metal surface atom and by forming a σ-backbond from the partially filled d_{xy} or d_{yz} metal orbitals to the antibonding π^* orbitals of O_2.
2. End-on adsorption through a single σ-type bond (Pauling model), in which the σ-orbital of O_2 donates electron to the d_{z^2} orbital on the metal.
3. Bridge model, with O_2 bonds with two sites, which was proposed by Yeager [42] principally for the reaction on platinum group metals.

In order to study the oxygen reduction mechanism, it is crucial to know the nature and coverage of adsorbed reaction intermediates. However, there is no simple adequate spectroscopic method for identifying adsorbed intermediates. Computational studies can provide insights regarding intermediates, their geometries, and energies. Anderson and Albu [30] carried out ab initio studies of reversible potentials and activation energies for uncatalyzed oxygen reduction to water and the reverse oxidation reaction. The electrode was modeled by a noninteracting electron-donor molecule with a chosen ionization potential (IP). When the reactant reached a point on the reaction path where its electron affinity (EA) matched the donor's IP, an electron transfer was assumed occurring, and the donor's IP or reactant's EA was identified with the electrode potential. To locate transition state, potential surface scan is deployed [43]. Once the transition state is located, the energy difference between the transition-state structure and reactants energy is taken as the activation energy. They calculated the activation energy of the following one-electron transfer steps:

$$O_2(g) + H^+(aq) + e^-(U) \rightarrow HO_2^{\bullet}(aq) \tag{11.9}$$

$$HO_2^{\bullet}(aq) + H^+(aq) + e^-(U) \rightarrow H_2O_2(aq) \tag{11.10}$$

$$H_2O_2(aq) + H^+(aq) + e^-(U) \rightarrow HO^{\bullet}(g) + H_2O(aq) \tag{11.11}$$

$$HO^{\bullet}(g) + H^+(aq) + e^-(U) \rightarrow H_2O(aq) \tag{11.12}$$

The MP2/6-31G** method is used. The $H^+(aq)$ was modeled with $H_3O^+(H_2O)_2$ cluster. The electron transfer was assumed to occur when the electron affinity of the reaction complex equaled the ionization potential, IP, of the electrode.

They studied activation energies for the four-electron transfer steps at potentials range between 0 and 2 V (vs. standard hydrogen electrode, SHE). The results showed that as the electrode potential increases, the activation barriers increase as well. The third electron and proton transfer step (Eq. 11.11), i.e., the H_2O_2 reduction, has the highest activation energy. Over the potential range they considered, activation energies for the reduction reactions decrease in the sequence: third step (Eq. 11.11) > first step (Eq. 11.9) > second step (Eq. 11.10) > fourth step (Eq. 11.12). From the calculation results, it is evident that an efficient four-electron reduction catalyst must not liberate hydrogen peroxide and it must activate the first and third reduction steps without deactivating the other two steps. Complete dissociation of HOOH on the electrode surface should lead to good activity, based on the low activation energy calculated for $HO^\bullet$ reduction.

In a subsequent study, Anderson and Albu [44] employed a similar method to study the catalytic effect of Pt on ORR. A single Pt atom is used to model the system. They calculated activation energies of the following four reduction steps:

$$\mathrm{Pt-O_2 + H^+(aq) + e^-}(U) \rightarrow \mathrm{Pt-OOH} \tag{11.13}$$

$$\mathrm{Pt-OOH + H^+(aq) + e^-}(U) \rightarrow \mathrm{Pt-OHOH} \tag{11.14}$$

$$\mathrm{Pt-OHOH + H^+(aq) + e^-}(U) \rightarrow \mathrm{Pt-OH + H_2O} \tag{11.15}$$

$$\mathrm{Pt-OH + H^+(aq) + e^-}(U) \rightarrow \mathrm{Pt-OH_2} \tag{11.16}$$

It is evident that the Pt atom has a significant catalytic effect on the most difficult step of the ORR, i.e., $H_2O_2 \rightarrow HO^\bullet + H_2O$. Activation energies drop about 1 eV over the 0–2 V potential range studied. Activation energies for the other reduction steps are also substantially reduced. The activation energies for $HO^\bullet$ reduction to H_2O increase when $HO^\bullet$ is bonded to the Pt atom and bonding to Pt decreases the activation energies for $OOH^\bullet$ reduction to H_2O_2. In all cases, the activation energies are predicted to increase with increasing potential (Fig. 11.4).

Sidik and Anderson further studied the O_2 electroreduction when bonded to Pt dual sites [45]. A Pt dimmer, Pt_2, with the bulk distance of 2.775 Å, was used to provide one- and twofold bonding sites for coordinating O_2, O, OOH, and OH. The results suggest that the O_2 on dual sites does not dissociate before the first electron transfer and the product for this step, OOH, easily dissociates with a small 0.06 eV activation barrier to form O and OH. The first electron transfer step has the highest activation barrier (0.60 eV at 1.23 V), which is close to the experimental value, and is predicted to be the rate-determining step.

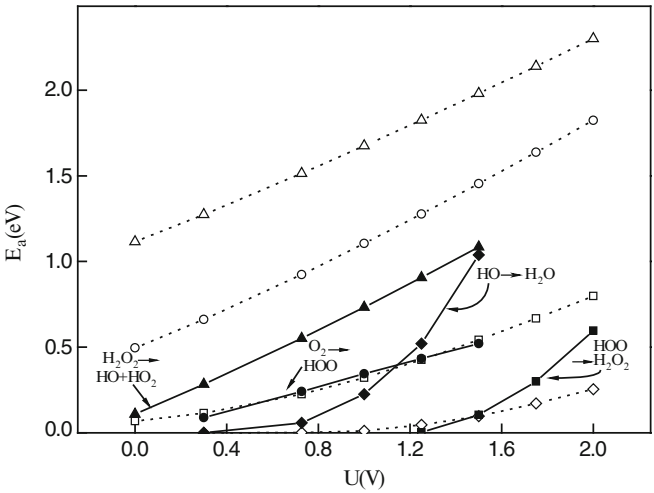

Fig. 11.4 Activation energy for the four steps of oxygen reduction to water as a function of electrode potential, *U*. *Heavy lines* connect points with species undergoing reduction bonded to a Pt atom. *Dotted lines* connect points with no bonding to the Pt. The same key applies to both sets of curves [44]

Li and Balbuena [46] used DFT method with B3PW91 functional, LANL2DZ effective core pseudopotentials for Pt, and 6-311G(d) basis set for O and H to study the first electron transfer step:

$$Pt_5 - O_2 + H^+(aq) + e^- \rightarrow Pt_5 - OOH \tag{11.17}$$

The solvent influence on the reaction is considered with $H_3O^+(H_2O)_2$ ion cluster model. It is found that the electron transfer process takes place gradually as the hydronium ion gets close to the adsorbed oxygen. The activation energies show a strong dependence on the $O_{ads}\cdots H\cdots O_{water}$ distance between the adsorbed oxygen and the proton water. The proton transfer reaction is not involved in the rate-determining step if the $O_{ads}\cdots H\cdots O_{water}$ distance is smaller than a certain threshold, which depends on the degree of proton solvation. Negatively charging the cluster/adsorbate complex causes a sharp decrease in the activation barrier.

Jinnouchi and Okazaki [47] performed AIMD studies of the first electron transfer reaction with one oxygen molecule, 1 hydronium ion, 9 water molecules, and 12 Pt atoms at 350 K. They proposed that the first reaction step would be rapid oxygen adsorption on the catalyst induced from the strong attractive force between the oxygen molecule and the platinum surface. The adsorbed water molecules and the hydronium ion hydrated the adsorbed oxygen atoms, and proton transfer through the constructed hydrogen bonds frequently occurred. When the conformation of these species satisfied certain conditions, the oxygen dissociation with the proton transfer reaction was induced, and three OH were generated on the platinum surface. The authors suggested that the generation of ordered cluster structure that

provides the effective path for ions and water molecules is the most important guiding principle for designing high ion conductive electrolytes.

11.4 ORR Catalyzed by Metal Catalysts

11.4.1 Platinum

Platinum has long been known as the best electrocatalyst for oxygen reduction in acidic medium [48]. The first step of catalyzing oxygen reduction involves chemisorption of oxygen molecule on the electrocatalyst surface. The adsorbate's structure, bonding type, and energy are key elements in understanding the effects of adsorption on the reaction kinetics. Theoretical studies of chemisorption of oxygen molecule can provide information about the nature of bonding at the surface, bond strength, geometry, and site preferences of adsorbates. Furthermore, theoretical calculations have advantage that the study can be performed for situations not realizable experimentally and can eliminate concerns about the effects of contaminants or other unknown variables.

Li and Balbuena [49] performed DFT calculation to study the interactions of oxygen with platinum clusters. They firstly calculated the ground-state structures of Pt_n clusters ($n = 4$–6). The results indicated that the structures for Pt_n clusters are nonplanar and most of them exhibit Jahn–Teller distortions. For atomic oxygen, a bridge-site adsorption is found as the most stable structure for Pt_3O. The adsorption energy for atomic oxygen shows a strong dependence on the metal cluster size and geometry. The bridge site is found to be the most favorable site for the adsorption of O_2 on Pt_n. In the dimer complexes Pt_2O_2, they found that the electron transferred from the Pt's *s* orbitals to the oxygen *p* orbitals, whereas in Pt_nO_2 ($n > 2$), the electron transferred from the Pt's *d* and *p* orbitals. The potential energy surface for the adsorption of oxygen shows a double well feature. The first potential energy minimum occurs at adsorption distances relatively far from the metal cluster. As the molecule gets closer to the cluster, the second minimum, which is more stable than the first one, appears corresponding to adsorbed state. A bond-order conservation approximation analysis illustrates that the dissociation activation energies depend on the Pt cluster size. The activation energies are reduced as the cluster's ionization potential (IP) decreases, which facilitates the charge transfer to the adsorbate. A similar effect on dissociation is observed upon application of an electric field along the direction of increase of the dipole moment of the adsorbate–cluster complex.

Similarly, Wang et al. [50] used B3LYP functional to study the adsorption and decomposition of the radical OOH and H_2O_2 on Pt clusters (Pt_3, Pt_4, Pt_6, and Pt_{10}). The potential energy surface for the complete reduction of oxygen in acidic medium has been calculated (Fig. 11.5). They found that the OOH radical has a very strong adsorption on Pt clusters. Both thermodynamics and kinetics indicate

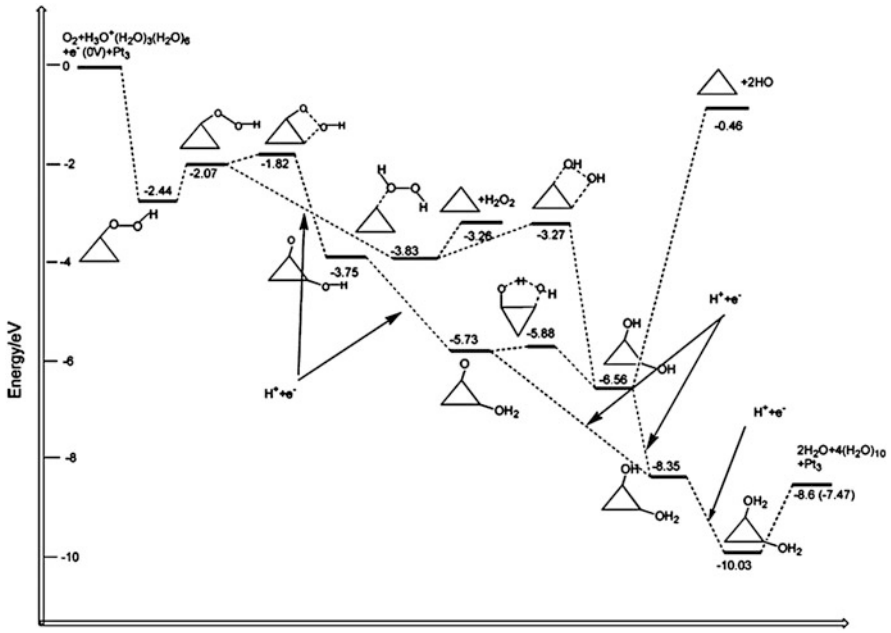

Fig. 11.5 Potential energy surface profile for the oxygen reduction reaction at the standard hydrogen electrode potential scale: the proton was modeled by two shells of water molecules, $H^+OH_2(H_2O)_3(H_2O)_6$, and the data in parentheses are Gibbs free energies [50]

that OOH readily decomposes into O and OH before a second electron transfer takes place. Thus, although a one-end adsorbed hydrogen peroxide H_2O_2, arising from the reduction of adsorbed OOH, has been located on Pt_3 and Pt_{10}, a favorable pathway for the second electron transfer should occur on the coadsorbed O and OH species, suggesting that O_2 reduction on a Pt surface may proceed via a *parallel* pathway: the *direct* (no H_2O_2 generated as intermediate) and *series* (H_2O_2 generated) occurring simultaneously, with the *direct* as the dominant step.

As discussed above, the oxygen adsorption and reduction processes are often simulated either on small Pt clusters or flat surfaces. However, both experimental measurements [51, 52] and computational calculations [53, 54] indicate that nanosized electrocatalysts show a considerably different catalytic activity from extended flat surfaces. These investigations would suggest that effects observed with particle size reduction go well beyond the increase in surface area and involve fundamental physical and chemical changes in the reaction steps. Han and his coworkers [55] studied explicitly Pt nanoparticles with 1 and 2 nm sizes and compared their chemical adsorption properties to those of an extended flat Pt (111) surface. As atomic oxygen (O) and hydroxyl group (OH) are two species of considerable importance [56], they focused on effect of particle size and Pt coordination on the chemisorption energies of O and OH.

Based on their calculations, the chemisorption energies of O and OH on the Pt (111) surface vary considerably from on that of 1 and 2 nm particles. With only sites near the center of the (111) facet on the 2 nm particle display similar adsorption energies to that of the Pt(111) bulk surface. While they find that on the bulk surface the fcc site is the most stable adsorption site, in agreement with previous work [57–59], oxygen adsorption is strongest at bridge sites on the edges of the 2 and 1 nm particles. For both particles, the maximal adsorption energy is larger than on the bulk surface. Depending on the location of sites, the adsorption energies at the fcc and hcp sites of the nanoparticles can be larger or small than that of the bulk surface value, with adsorption getting stronger as the site location getting closer to the edge of the surface.

While, in general, the adsorption energy on the 1 nm particle on equivalent sites is higher than on the 2 nm particle, this trend is reversed for the fcc (111) site. This peculiarity is attributed to the significant curvature on the surface of 1 nm particle in order to reduce the total surface area of the particle. This causes the distance between nearest neighbor Pt atoms to be longer on the surface of the 1 nm particle (2.85 Å) than on the 2 nm particle (2.7 Å). This bond elongation prevents the effective interaction between oxygen and the three Pt atoms defining the site.

The effect of particle size on adsorption energy and catalytic activity is complex. It depends on the precise role that the adsorbed species play in the catalytic process and on the change in adsorption of other relevant species. Watanabe et al. [60] argued that particle size has no effect on the rate of the ORR; however, the mean particle spacing on the support is the more relevant variable though his findings have been disputed by Giordanoa et al. [61] and Takasu et al. [62]. Similarly, Yano et al. [63] studied the ORR catalytic activity and the ratio of peroxide (H_2O_2) formation on Pt particles with 1.6, 2.6, and 4.8 nm in diameter. By NMR analysis of ^{195}Pt located at surfaces of the Pt nanoparticles, they found that the electronic structure of Pt does not change with particle size, from which they concluded that the ORR activity does not change with Pt particle size. Mayrhofer et al. [64], on the other hand, argued that the rate of the ORR decreases with decreasing in particle size as stronger OH adsorption blocks oxygen adsorption sites. Based on the analysis above, the authors concluded that there might be no general relationship between the particle size and the catalytic activity. Nevertheless, clever engineering of nanostructure of catalyst materials to optimize the adsorption strength and increase number of adsorption sites for the intermediate species involved could, in principle, be used to fabricate better electrocatalysts. Certainly such an approach would require a better understanding of reaction mechanism and effect of nanostructure on adsorption of various intermediate species.

11.4.2 Platinum-Based Metal Catalysts

The polarization in a PEMFC comes mainly from the slow cathodic ORR. Reducing the Pt loading (particularly in the cathode catalyst layer) without compromising

fuel cell performance is a strategy to meet the cost reduction requirements for PEMFC commercialization [65, 66]. In other words, the design of novel catalysts requires not only reducing the amount of Pt used but also enhancing catalytic activity and stability [67]. Several approaches have been developed to address reduction of Pt loading, including (1) improving nanostructures to increase the surface-to-volume ratio of catalyst materials [68]; (2) using an alloying technique to incorporate non-precious metals into the nanostructures; and (3) texturing nanostructures, e.g., replacing the core atoms in Pt nanoparticles with a non-precious metal, resulting in a Pt-skin [69, 70] or Pt monolayer catalysts [71–73].

Several Pt-based bimetallic systems have been reported showing good ORR activity. For instance, alloying Pt with transition metals such as Co [74, 75], Ni [76–78], Fe [79], Mn [79], Cr [80–82], and V [83] is highlighted as a promising approach toward improving ORR electrocatalysis in acidic solutions. A number of explanations have been proposed for the observed improvement in activity by the addition of a less noble metal to Pt [84]. These include the lower oxidation state of the Pt which can suppress Pt oxide formation, a shortening of Pt–Pt interatomic distance and therefore a more favorable adsorption of O_2 (geometric effect), an increased *5d*-orbital vacancies (electronic effect), and formation of a thin Pt skin on the surface of the alloy [85] which has unusual electronic properties. Using the conventional Pt/C catalyst as the baseline, the ORR activities of PtM alloys (M = Ni, V, Co, and Fe) follow the order: Pt/C < PtNi/C < PtV/C < PtCo/C < PtFe/C [86–88].

Wang et al. [89] carried out first-principle DFT calculations to investigate how a subsurface transition metal M (M = Ni, Co, or Fe) affects the energetics and mechanisms of ORR on the outermost mono-surface layer of Pt/M(111). With the calculation, they illustrated that the subsurface Ni, Co, and Fe could downshift the *d*-band center of the Pt surface and thus weaken the binding of chemical species to the Pt/M(111) surface. Moreover, the subsurface Ni, Co, and Fe could modify the heat of reaction and activation energy of various elementary reactions of ORR. The results revealed that, due to the influence of the subsurface Ni, Co, or Fe, ORR would adopt a hydrogen peroxide dissociation pathway. The activation energy for the rate-determining O_2 protonation reaction is 0.15, 0.17, and 0.16 eV on Pt/Ni (111), Pt/Co(111), and Pt/Fe(111), respectively. In contrast, the activation energy for the same reaction on a pure Pt(111) surface is 0.79 eV. The theoretical study explained why the subsurface Ni, Co, and Fe could lead to multifold enhancement in catalytic activity of ORR on the Pt/M(111) catalysts.

Xu et al. [57] performed self-consistent periodic DFT calculations (GGA–PW91) to study the adsorption of O and O_2 and the dissociation of O_2 on the (111) facets of ordered Pt_3Co and Pt_3Fe alloys and on monolayer Pt skins covering these two alloys. They also investigated explicitly the strain effect by a 2 % compression of Pt(111). They discovered that the Co atoms on the $Pt_3Co(111)$ surface allow O_2 to dissociate more easily than on Pt(111) [the lowest activation energy on $Pt_3Co(111)$ is 0.24 eV/O_2, compared to 0.77 eV/O_2 on Pt(111)] and also bind O and O_2 more strongly (−4.29 eV/O vs. −3.88 eV/O, −0.92 eV/O_2 vs. −0.62 eV/O_2). While for monolayer Pt-skin catalysts, the authors showed that

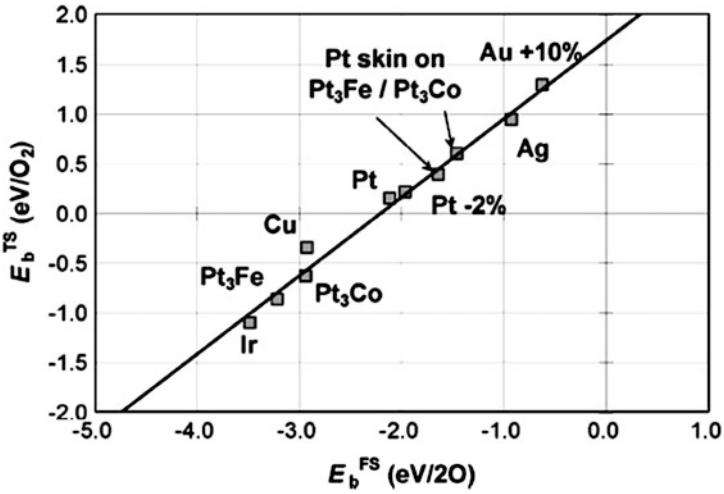

Fig. 11.6 Binding energies of the transition states of O_2 dissociation (E_b^{TS}) vs. binding energies of the atomic final states with respect to gas-phase O_2 (E_b^{FS}) on the (111) facets of several fcc transition metals and alloys [57]

although these catalysts are less reactive than pure Pt for O_2 dissociation, they are more active toward the ORR because they are less poisoned by O and facilitate the activation of O and O-containing intermediates in bond-making elementary reaction steps in the ORR.

The authors also revealed that there is a linear relationship between atomic oxygen binding energy and the oxygen dissociation barrier of the transition metals and alloys (Fig. 11.6). The more strongly a material binds atomic oxygen, the more effective it will be in dissociating molecular oxygen. So instead of conducting a complicated and expensive transition-state study, a more affordable atomic binding study can be used to screen and design better oxygen reduction catalysts.

Mavrikakis et al. [90] performed spin-polarized DFT calculations to study the ORR catalytic activity of platinum monolayers supported on close-packed transition metal surfaces [(Au(111), Pt(111), Pd(111), and Ir(111)]. To estimate the relative activity of these catalysts at two different cell potentials (1.23 and 0.80 V), both the free-energy changes and activation energy barriers for elementary reactions are calculated. They observed that OH removal is the rate-limiting step for ORR at the potential of 1.23 V. At a cell potential of 0.80 V, the proton/electron transfer steps become easier, and Pt*/Pd shows the highest activity among the surfaces examined, even higher than that of pure Pt(111). The activity of the other two surfaces, namely, Pt*/Au and Pt*/Ir, is lower due to the difficulty in OH removal and in O–O bond scission, respectively. Their findings provide additional insights into the ORR mechanism for these supported platinum monolayer surfaces.

11.4.3 Other Metal Catalysts

Palladium-alloy materials have been recently introduced as a promising ORR cathode electrocatalyst for replacing Pt [91–98]. Pd alloys are considerably less expensive than Pt. Besides, experimental studies indicate that they have high methanol tolerance for direct methanol fuel cells (DMFCs) in which the methanol crossover to the cathode significantly decreases the cell's efficiency [99, 100].

Shao et al. [101] measured the ORR activity of Pd monolayers supported on Ru (0001), Rh(111), Ir(111), Pt(111), and Au(111) using the rotating disk electrode technique and correlated the findings with the *d*-band center of Pd calculated from DFT method. They observed the activity of Pd monolayers supported on Ru(0001), Rh(111), Ir(111), Pt(111), and Au(111) increased in the following order: Pd/Ru (0001) < Pd/Ir(111) < Pd/Rh(111) < Pd/Au(111) < Pd/Pt(111). A volcano-type dependence of activity on the energy of the *d*-band center of Pd monolayers was found, with Pd/Pt(111) at the top of the curve. They also synthesized a Pd_2Co/C alloy, and the results showed that the non-Pt alloy's ORR activity is comparable to that of commercial Pt-based catalysts. The kinetics of the ORR catalyzed by this electrocatalyst predominantly involves a four-electron reduction with the first electron transfer being the rate-determining step. The downshift of the *d*-band center of the Pd "skin," which constitutes the alloy surface due to the strong surface segregation of Pd at elevated temperatures, contributed to its high ORR activity. Additionally, the catalyst showed very high methanol tolerance, retaining very high catalytic activity for the ORR at high concentrations of methanol.

Very recently, Erikat et al. [102] used periodic self-consistent DFT calculations to study the adsorption and the reaction barrier for the dissociation of O_2 on Ir(100) surface. Dissociative adsorption is found to be energetically more favorable than molecular adsorption. Among all the cases studied, parallel approaches (*Prl*1 and *Prl*2) on a hollow site, with the same adsorption energy of −3.93 eV, are found to be the most energetically preferred sites of adsorptions. Hybridization between *p*-O_2 and *d*-metal orbitals is responsible for the dissociative adsorption. By using the nudge elastic band method (NEB), they found that the dissociation occurs immediately and very early along the dissociation path with a small activation barrier (0.26 eV).

Through DFT slab calculations, the adsorption and dissociation of O_2 on CuCl (111) surface have been systematically studied by Zhang et al. [103]. Different modes of atomic O and molecular O_2 adsorption on CuCl(111) surface and possible dissociation pathways are examined; vibrational frequency and Mulliken charge are also calculated. Their results showed that the favorable adsorption occurs at hollow site for O atom and molecular O_2 lying flatly on the surface with one O atom on top of Cu atom is the most stable adsorption configuration. The O–O stretching vibrational frequencies are significantly red-shifted, and the charges are transferred from CuCl to oxygen. Upon O_2 adsorption, adsorbed species on CuCl(111) surface exhibit the characteristic of the superoxo (O_2^-), which contributes to improving the catalytic activity of CuCl. Meanwhile, O_2 dissociation into atomic O could also occur; however, it needs to overcome a very large activation barrier.

11.5 Non-precious Metal Catalysts

At the current technology stage, Pt-based electrocatalysts are the most practical materials in terms of both activity and stability, although their performance is still insufficient and needs further improvement. The major drawback of these Pt-based catalysts is the limited availability and high cost, contributing to the excessive production costs of fuel cell systems.

The search for inexpensive, high-performance electrocatalysts has taken two different approaches. The first approach is to reduce catalyst usage through increasing Pt utilization in the catalyst layers. This can be achieved by alloying Pt with inexpensive metals (Co, Fe, etc.) and/or by utilizing unique support materials for thin-layer Pt nanoparticle deposition. In the last two decades, the required Pt loading has been reduced significantly to approximately 0.4 mg cm^{-2} [104]. Unfortunately, the increasing of Pt price during the same time has totally offset the Pt loading reduction, rendering the efforts toward Pt loading reduction ineffective. Therefore, this approach may not be a viable solution for cost reduction of PEMFC. The other approach is to develop non-precious metal-based electrocatalysts. Although the performance of the non-precious metal catalysts (carbon-supported Fe– and/or Co–N catalysts) is still inferior to Pt-based catalysts in terms of both activity and stability, in the last few years, significant progress has been made in the development of non-precious metal catalysts making it one of the most active and promising research areas [105].

Non-precious metal catalyst research covers a broad range of materials. The most promising catalysts investigated thus far are carbon-supported M–N_x/C materials (M = Co, Fe, Ni, Mn, etc.) formed by pyrolysis of a variety of metal, nitrogen, and carbon precursor materials [106]. Other non-precious metal electrocatalyst materials investigated include non-pyrolyzed transition metal macrocycles [107–122], conductive polymer-based complexes (pyrolyzed and non-pyrolyzed) [123–140], transition metal chalcogenides [141–148], metal oxide/carbide/nitride materials [149–166], as well as carbon-based materials [167–179]. The advances of these types of materials can be found in Chaps. 7–10 and 12–15 of this book.

To meet the need of PEMFC, increasing volumetric density of non-precious metal catalysts is required; however, without knowledge of active-site structure, it is very challenging to increase the active-site density. There are many challenges in determining the active-site structures. There is lack of adequate material characterization techniques. The active sites may be scarce. Furthermore, different active sites may contribute to the catalytic activity of the materials [180]. There are different reviews regarding the nature of active sites. One school believes that metal is at the active sites, while the other believes that metal merely catalyzes the formation of active sites from carbon, nitrogen, and perhaps oxygen atoms [181–184]. Some researchers believe that the ORR activity is originated from the formation of graphitic nitrogen and/or pyridinic nitrogen functional groups. This claim has been supported in the literature with ORR activity of metal-free N/C catalyst materials [185, 186]. This further demonstrates the convoluted understanding

regarding the exact nature of the catalytically active moieties with respect to ORR. First-principle modeling is a valuable tool in exploring active-site structures and providing insights into the reaction mechanism.

11.5.1 Transition Metal Macrocycle Catalysts

Transition metal macrocycle compounds have been employed as ORR catalysts since the first study by Jasinski in 1964 [187]. The activity of these complexes has been found to be directly related to the metal ion center and encompassing ligand structure [105]. Simple cobalt-based complexes (i.e., cobalt phthalocyanines or cobalt porphyrins) have catalytic activity toward the reduction of oxygen by a two-electron process to produce H_2O_2, whereas a four-electron reduction process forming H_2O is commonly observed for Fe-based complexes. Although the activity of unpyrolyzed transition metal macrocycle catalysts is inferior to its pyrolyzed counterpart, the major benefit of studying non-pyrolyzed macrocyclic catalyst is for fundamental understanding, as the active sites of these catalysts are well known, which allows a direct link between the catalyst structure and its ORR activity. Thus, theoretical studies have been conducted to understand the relationship between the transition metal macrocyclic complex structures and their electrocatalytic properties.

Sun et al. [188] performed DFT calculation to study the electrochemical reduction mechanism of oxygen on four metal macrocyclic complexes, iron phthalocyanines (FePc), iron porphyrin (FeP), cobalt phthalocyanine (CoPc), and cobalt porphyrin (CoP). Based on their calculation results, for the four metal macrocyclic complexes, O_2 will not directly be cleaved without the cooperation of hydrogen. In the reduction process, with FePc or FeP as catalyst, O_2 is reduced to H_2O ($4e^-$ transfer) without the formation of intermediate H_2O_2, while on CoPc or CoP, O_2 is reduced to H_2O_2 ($2e^-$ transfer). The authors attributed the four-electron reduction capability of Fe complexes to their high-lying HOMO of these complexes (see Fig. 11.7), which make the electron donation to oxygen easier; as a result, more electron are transferred to O–O antibonding orbital, and O–O bond is readily broke.

Shi and Zhang [189] carried out DFT calculations to study the dioxygen-binding abilities on the following iron and cobalt systems: CoPc (cobalt phthalocyanine), $CoF_{16}Pc$ (cobalt hexadecafluorophthalocyanine), CoMeOPc (cobalt octamethoxyphthalocyanine), CoTSPc (cobalt tetrasulfophthalocyanine), CoTNPPc (cobalt tetraneopentoxyphthalocyanine), CoP (cobalt porphyrin), CoTPP (cobalt tetraphenylporphyrin), CoTPFPP (cobalt tetrakis(pentafluorophenyl)porphyrin), FePc, $FeF_{16}Pc$, FeMeOPc, FeTSPc, FeTPyPz (iron-2,3-pyridinoporphyrazine) FeP, FeTPP, and FeTPFPP. The ionization potential of the above metal macrocyclic complexes was also calculated.

Their calculations demonstrated that dioxygen-binding abilities of the transition metal macrocyclic complexes are determined by central metal, ligand, and substituents. For cobalt phthalocyanine systems, electron-donating substituents increase

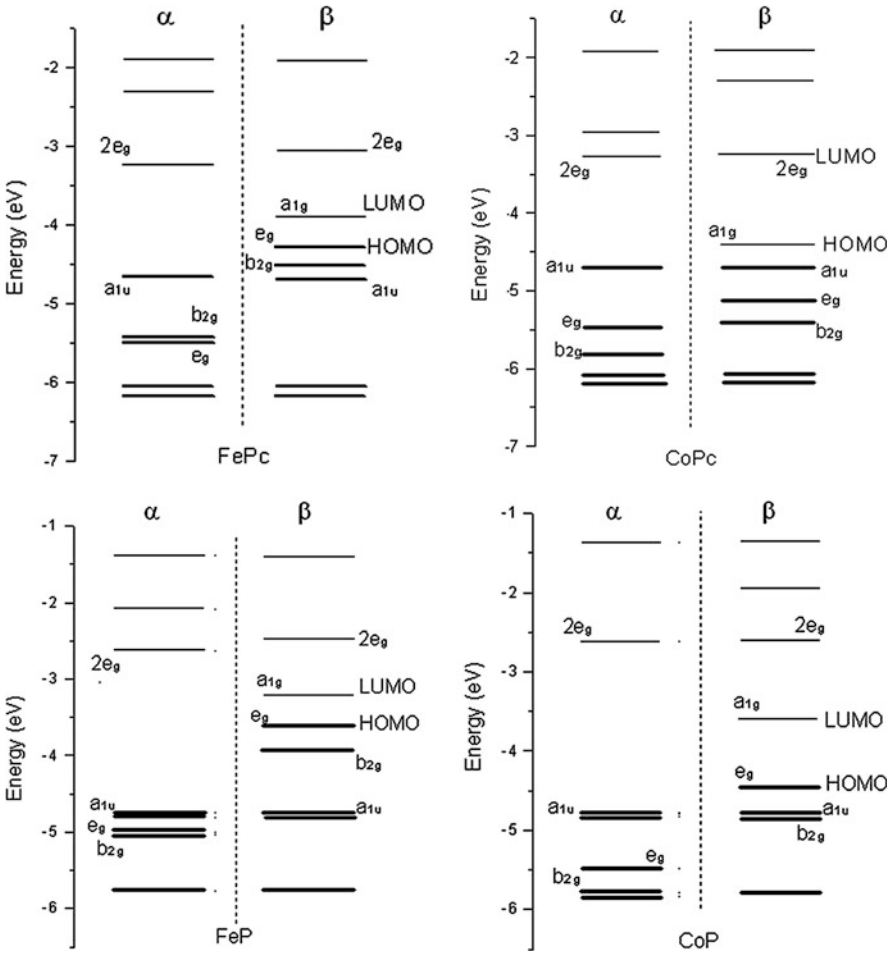

Fig. 11.7 Energy levels of MPc and MP (M = Fe, Co, α = spin-down orbital, β = spin-up orbital) [188]

its dioxygen-binding ability, and electron-withdrawing substituents decrease the dioxygen-binding ability of the systems. In general, the transition metal macrocyclic systems' ORR catalytic activity is related to its ionization potential and dioxygen-binding ability. Higher ionization potential and larger dioxygen-binding energy are associated with better catalytic activity. For porphyrin systems, cobalt derivatives have higher ionization potential and higher reactivity. For phthalocyanine systems, iron derivatives have good ionization potential and large oxygen-binding energy.

Similarly, Li et al. [190] investigated the interaction between dioxygen and various iron macrocyclic complexes (Fig. 11.8) by means of first-principle calculations. Their results indicated that the macrocyclic ligands without aromaticity were better electron-donor ligands, facilitating the backbonding from iron to O_2

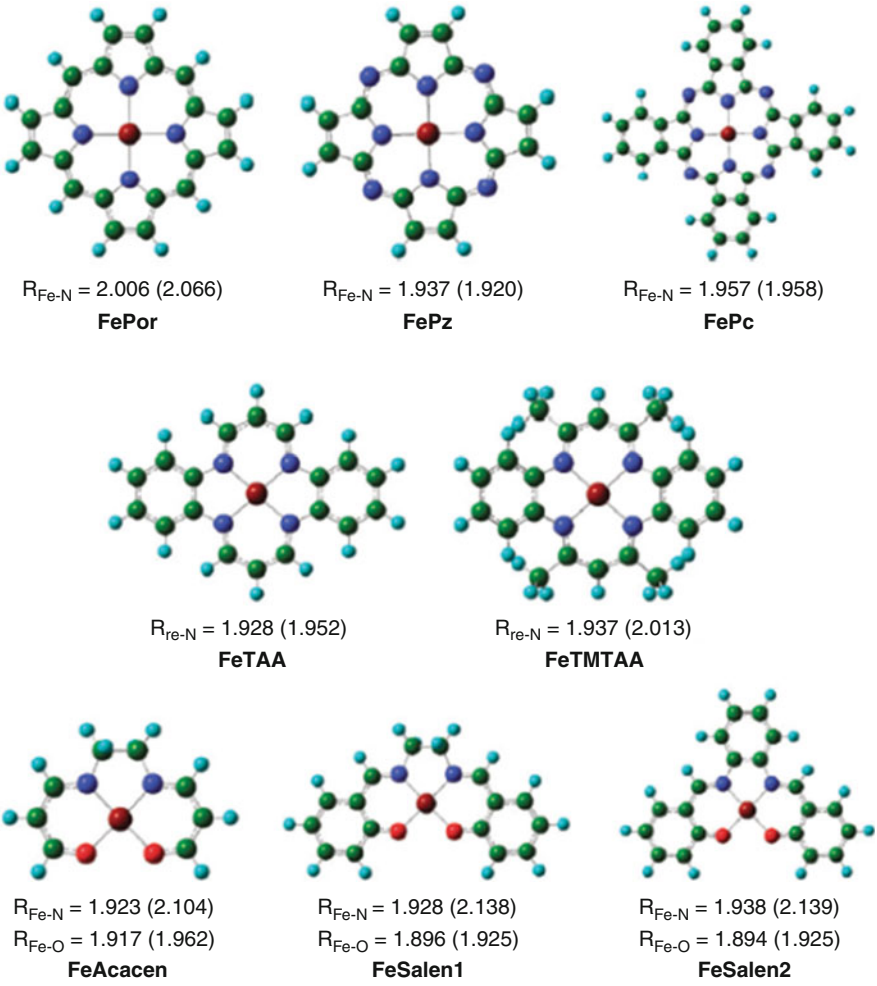

Fig. 11.8 The structures for the deoxy-systems (FeX) under study. The *maroon balls* are iron atoms, the *blue balls* are nitrogen atoms, the *red balls* are oxygen atoms, the *green-black balls* are carbon atoms, and the *turquoise balls* are hydrogen atoms. R_{Fe-N} is the distance (Å) between the Fe and the coordinated nitrogen atom, and R_{Fe-O} is the distance between the Fe and the coordinated oxygen atom. Data out of the parentheses are for the triplets, in the parentheses for the quintets [190]

and activated O_2 more significantly. Furthermore, the activation of O_2 was closely related to the energy of the HOMO of iron macrocyclic complexes. The smaller the energy gap between the HOMO of iron macrocyclic complexes and the LUMO of dioxygen, the more reactive the adsorbed O_2 became, with a longer O–O bond distance and a shorter Fe–O bond length. Based on their study, the authors proposed that FeTMTAA is a potential catalyst in oxidation reactions using O_2 as oxidant. FeAcacen, FeSalen1, and FeSalen2 are also promising catalysts for oxidation

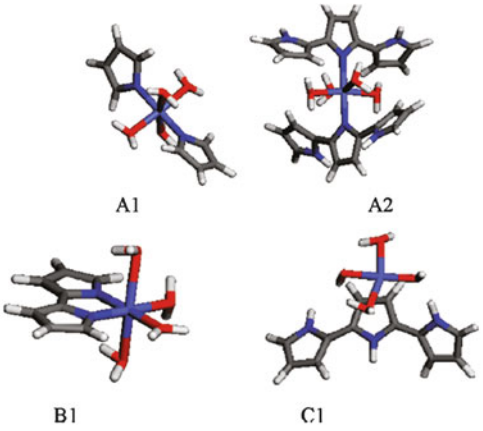

Fig. 11.9 Optimized structures of four proposed active sites [193]. *Blue*: Co, *dark blue*: N, *gray*: C, *white*: H, *red*: O

reactions. Furthermore, by modifying the structure of iron macrocyclic complexes through substituent groups and axial ligand, the ORR catalytic efficiency could be tuned.

11.5.2 Conductive Polymer-Based Complex Catalysts

Conductive polymers such as polypyrrole (PPy), polyaniline (PAni), and polythiophen (PTh) have been the subject of much research owing to their wide applications in biosensors, electrochemistry, and electrocatalysis [191, 192]. Recently, conductive polymers have been also investigated as ORR electrocatalysis in three different ways: (1) utilizing conductive polymers as ORR electrocatalysts on their own, (2) incorporating non-precious metal complexes into the conductive polymer matrix, and (3) employing conductive polymers as a nitrogen/carbon precursor material for pyrolyzed M–N_x/C catalysts [105].

Shi et al. [193] employed DFT and experimental characterization to investigate active-site structures of unpyrolyzed cobalt–polypyrrole (Co–PPy) composites. They specifically examined four types of the active-site structures and studied the stability of each structure. They also examined oxygen adsorption on these structures with both end-on and side-on configurations and calculated the redox potential of each structure (Fig. 11.9). The theoretical simulations indicated that various active-site structures could contribute to the ORR activity of non-heat-treated Co–PPy catalysts and both Co(III) and Co(II) could play the role of an active center. The active site's oxygen binding strength (end-on or side-on) dictates its dominant reaction pathway ($2e^-$ or $4e^-$). With calculated redox potential of each active site and its oxygen binding strength, each active site's contribution to $2e^-$ or $4e^-$ pathway at a defined potential can be deduced. Base on their results, the studied active sites contributed more to $2e^-$ pathway at low potential (0.3 V vs. RHE) than that at high potential (0.6 V vs. RHE), which is consistent with experimental

observed change of hydrogen peroxide formation at different potentials. The calculations illustrated that more than one type of active sites contribute to the ORR activity observed with untreated cobalt–polypyrrole catalysts. Type A structures give similar potential dependence hydroperoxide formation trend as that observed from experiment. They postulated that for untreated Co–PPy composites, the presence of the type A structures is likely.

Another insight provided by their study is that the side-on oxygen adsorption requires more space than the end-on adsorption configuration. This may be one of the reasons why cobalt porphyrin and phthalocyanine systems cannot form stable side-on adducts which generally lead to $4e^-$ transfer products. The destruction of the ordered structure of such a macrocyclic catalyst during the heat treatment is likely to increase the number of sites that facilitate the side-on oxygen adsorption, and this leads to an increase in the number of electrons transferred in the ORR.

Similarly, the interaction between the oxygen molecule and Co–(*n*)pyrrole model clusters ($n = 4, 6$) was recently studied by Dipojono et al. [194, 195]. The stable adsorption site of the O_2 molecule on Co–(4)pyrrole is found to be in a side-on configuration, while for the case of Co–(6)pyrrole cluster, the O_2 molecule is slightly deviated from the side-on configuration. The O–O bonds of the O_2/Co–(4)pyrrole and the O2/Co–(6)pyrrole systems have elongated by 11.84 and 9.86 %, respectively. The elongation mechanism of O_2 on Co–(*n*)pyrrole is induced by the interaction between the cobalt *d*-orbitals and the O_2 antibonding π^* orbital, which results in a charge transfer from the cobalt atom toward the O_2 molecule. In Co–(4)pyrrole, the elongation of the O_2 bond is larger than that of Co–(6)pyrrole since a complete side-on configuration has more symmetric overlapping between the cobalt *d*-orbitals and the O_2 antibonding orbital. Furthermore, the dissociation energy is affected by the amount of the charge transferred from Co–(*n*)pyrrole clusters to the O_2 molecule in the transition state.

11.5.3 Carbon-Based Materials

Carbon-based materials with large surface area such as carbon nanotubes, nanofibers, and graphene have recently received attention as potential metal-free catalyst materials for ORR [167–179]. In particular, nitrogen (N)-doped carbon materials have been shown to yield high ORR activity with four-electron transfer mechanism [167, 169]. Matter et al. [173] reported that the N-doped carbon nanofibers have high ORR catalytic activity and the N-doped nanotubes and graphene [170] were also recently reported to have high activity for ORR in the absence of transition metal atoms. The pyridinic N site (nitrogen atoms with lone pair electrons) has been generally considered as catalytic active site for ORR due to delocalizing of π electrons to pyridinic N, and existence of a large amount of pyridinic nitrogen is usually observed with highly active carbon materials [169, 170, 172]. On the contrary, a recent experiment suggested that the graphitic N (nitrogen bonded to three sp^2 carbon atoms) was the key for ORR activity rather

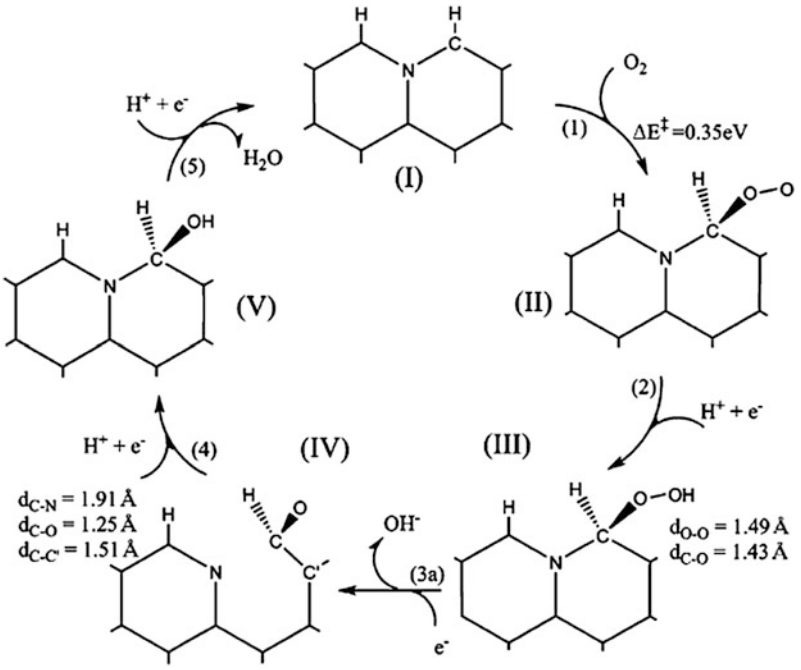

Fig. 11.10 The proposed ORR catalytic cycle [198]

than pyridinic N [196]. It is, in fact, difficult to distinguish the edge vs. pyridinic N experimentally [197], as graphitic N at edge can become a pyridinic N.

In order to elucidate the active sites for N-doped graphene materials, Jung et al. [198] performed the spin-polarized DFT calculations of graphene nanoribbon edges. They observed that the nitrogen doping increases the activity of graphene edges by enhancing the first electron transfer and giving dominate four-electron reduction products, which are the two most important aspects for improving ORR selectivity and performance. The outermost graphitic nitrogen site among others yields the lowest barrier for the rate-limiting first electron transfer as well as the highest selectivity toward the four-electron reduction pathway and hence is proposed to be the primary active site. Furthermore, the proposed catalytic cycle (Fig. 11.10) involves a ring opening of the cyclic C–N bond at the edge of graphene which converts the graphitic N to pyridinic N. This interconversion of graphitic to pyridinic N may reconcile the controversy regarding pyridinic or graphitic nitrogen as the ORR active sites for N-doped graphene materials.

Functionalized graphitic materials with late transition metals were recently studied by Rossmeisl et al. [199]. They showed that graphitic materials with active sites composed of four nitrogen atoms and transition metal atoms belonging to groups 7–9 in the periodic table are active toward ORR. Spin analyses suggested that the oxidation state of those elements in the active sites is, in general, +2. Moreover, their results showed that transition metals do not have intrinsic catalytic

activities, since their adsorption behavior can be severely altered by changes in the local geometry of the active site, the chemical nature of the nearest neighbors, and the oxidation states. Furthermore, the catalytic performance of ORR can be improved by stabilizing the adsorption of OOH with respect to that of OH, which can be achieved by carefully engineering the active sites.

Yu et al. [200] performed periodic DFT calculations to study the ORR catalyzed by N-graphene. The study took the solvent, surface adsorbates, and surface coverage into consideration. They observed that it is essential to include water effect in constructing a reliable free-energy reaction profile, especially for O_2 adsorption which is significantly enhanced by the polarization of O_2 in the presence of water due to hydrogen bond formation. Without water, O_2 cannot be adsorbed on the N-graphene surface. The formation of OOH^- is found to be energetically unfavored compared with the dissociation reaction $OOH_{(ads)} \rightarrow O_{(ads)} + OH^-$. The result suggests that O_2 is mainly reduced via a "$4e^-$ reduction" pathway on N-doped graphene. The rate-determining step is the removal of $O_{(ads)}$ from the N-graphene surface. Thus, they suggested that a catalyst with a high efficiency in $O_{(ads)}$ removing should have a high activity.

11.6 Conclusions

Past few years or so have witnessed a big increase of theoretical modeling studies in electrocatalyst materials. These studies are enabled by better computational algorithms and fast computational facilities and fueled by the demand of environmental friendly and sustainable energy resources. Theoretical modeling complementing experimental study has shed light on detailed surface phenomena, formation of intermediates, and the activation energies related to elementary reaction steps and provided better understanding of ORR mechanisms. Methodologies that employ structure activity relationship such as adsorption energy, activation energies, and *d*-band centers have shown encourage results in identifying better electrocatalysts. They are invaluable tools to screen for better electrocatalysts. On the other hand, due to its limitation with simple model and small-sized systems, first-principle methods have difficulty in providing quantitative numbers for detailed reaction steps. The major issue with theoretical study of ORR in PEMFC is how to model the interface effectively. Better models and methodologies need to be developed to study electrochemical systems. More theoretical studies are needed to provide better understanding of ORR and to help design novel electrocatalysts.

References

1. Jacobson MZ, Colella WG, Golden DM (2005) Cleaning the air and improving health with hydrogen fuel-cell vehicles. Science 308(5730):1901–1905
2. Dusastre V (2001) Materials for clean energy. Nature 414(6861):331

3. Bashyam R, Zelenay P (2006) A class of non-precious metal composite catalysts for fuel cells. Nature 443(7107):63–66
4. EG&G Technical Services Inc (2004) Fuel cell handbook. 7th ed. Morgantown, West Virginia: National Energy Technology Lab, US Department of Energy
5. Shi Z, Zhang J, Liu ZS, Wang H, Wilkinson DP (2006) Current status of ab initio quantum chemistry study for oxygen electroreduction on fuel cell catalysts. Electrochim Acta 51(10): 1905–1916
6. Xu H, Kunz R, Fenton JM (2007) Investigation of platinum oxidation in PEM fuel cells at various relative humidities. Electrochem Solid State Lett 10(1):B1–B5
7. Holby EF, Greeley J, Morgan D (2012) Thermodynamics and hysteresis of oxide formation and removal on platinum (111) surfaces. J Phys Chem C 116(18):9942–9946
8. Appleby AJ (1993) Electrocatalysis of aqueous dioxygen reduction. J Electroanal Chem 357(1–2):117–179
9. Markovic NM, Ross PN Jr (2002) Surface science studies of model fuel cell electrocatalysts. Surf Sci 45(4–6):117–229
10. Schmickler W (1999) Recent progress in theoretical electrochemistry. Annu Rep Prog Chem Sect C Phys Chem 95:117–162, Chapter 5
11. Grimbolt J, Luntz AC, Fowler DE (1990) Low temperature adsorption of O_2 on Pt (111). J Electron Spectrosc Relat Phenom 52:161–174
12. Luntz AC, Williams MD, Bethune DS (1988) The sticking of O_2 on a Pt(111) surface. J Chem Phys 89(7):4381–4395
13. Stohr J, Gland JL, Eberhard W, Outka D, Madix RJ, Sette F, Koestner RJ, Doebler U (1983) Bonding and bond lengths of chemisorbed molecules from near-edge X-ray-absorption fine-structure studies. Phys Rev Lett 51(26):2414–2417
14. Sexton BA (1981) Identification of adsorbed species at metal-surfaces by electron-energy loss spectroscopy (EELS). Appl Phys A 26(1):1–18
15. Wurth W, Stohr J, Feulner P, Pan X, Bauchspiess KR, Baba Y, Hudel E, Rocker G, Menzel D (1990) Bonding, structure, and magnetism of physisorbed and chemisorbed O_2 on Pt (111). Phys Rev Lett 65(19):2426–2429
16. Puglia C, Nilsson A, Hernnas B, Karis O, Bennich P, Martensson N (1995) Physisorbed, chemisorbed and dissociated O_2 on Pt(111) studied by different core level spectroscopy methods. Surf Sci 342(1–3):119–133
17. Keith JA, Jacob T (2010) Computational simulations on the oxygen reduction reaction in electrochemical. In: Balbuena PB, Subramanian VR (eds) Theory and experiment in electrocatalysis. Springer, New York, pp 89–132
18. Koper MTM (2003) Ab initio quantum-chemical calculations in electrochemistry. In: Vayenas CG, Conway BE, White RE (eds) Modern aspects of electrochemistry, vol 36. Kluwer/Plenum, New York, Chapter 2
19. Kohn W, Sham LJ (1965) Self-consistent equations including exchange and correlation effects. Phys Rev 140(4A):A1133–A1138
20. Becke AD (1988) Density-functional exchange-energy approximation with correct asymptotic behavior. Phys Rev A 38(6):3098–3100
21. Kohanoff J, Gidopoulos NI (2003) Density functional theory: basics, new trends and applications. In: Wilson S (ed) Handbook of molecular physics and quantum chemistry, vol 2. Wiley, Chichester, pp 532–568, Part 5, Chapter 26
22. Perdew JP (1986) Density-functional approximation for the correlation-energy of the inhomogeneous electron-gas. Phys Rev B 33(12):8822–8824
23. Perdew JP, Chevary JA, Vosko SH, Jackson KA, Pederson MR, Singh DJ, Fiolhais C (1992) Atoms, molecules, solids, and surfaces-applications of the generalized gradient approximation for exchange and correlation. Phys Rev B 46(11):6671–6687
24. Perdew JP, Wang Y (1992) Accurate and simple analytic representation of the electron-gas correlation-energy. Phys Rev B 45(23):13244–13249
25. Becke AD (1993) Density-functional thermochemistry. III. The role of exact exchange. J Chem Phys 98(7):5648–5652

26. Lee C, Yang W, Parr RG (1988) Development of the colle-salvetti correlation-energy formula into a functional of the electron-density. Phys Rev B 37(2):785–789
27. Becke AD (1993) A new mixing of Hartree-Fock and local density-functional theories. J Chem Phys 98(2):1372–1377
28. Perdew JP, Burke K, Ernzerhof M (1996) Generalized gradient approximation made simple. Phys Rev Lett 77(18):3865–3868
29. Albu TV, Mikel SE (2007) Performance of hybrid density functional theory methods toward oxygen electroreduction over platinum. Electrochim Acta 52(9):3149–3159
30. Anderson AB, Albu TV (1999) Ab initio determination of reversible potentials and activation energies for outer-sphere oxygen reduction to water and the reverse oxidation reaction. J Am Chem Soc 121(50):11855–11863
31. Adamo C, Barone V (1998) Exchange functionals with improved long-range behavior and adiabatic connection methods without adjustable parameters: the mPW and mPW1PW models. J Chem Phys 108(2):664–675
32. Becke AD (1996) Density-functional thermochemistry. IV. A new dynamical correlation functional and implications for exact-exchange mixing. J Chem Phys 104(3):1040–1046
33. Car R, Parrinello M (1985) Unified approach for molecular-dynamics and density-functional theory. Phys Rev Lett 55(22):2471–2474
34. Grotendorst J, Blügel S, Marx D (eds) (2006) Computational nanoscience: do it yourself! vol 31, NIC Series. John von Neumann Institute for Computing, Jülich, pp 195–244
35. Tse JS (2002) Ab initio molecular dynamics with density functional theory. Annu Rev Phys Chem 53:249–290
36. Yeager E (1984) Electrocatalysts for O_2 reduction. Electrochim Acta 29(11):1527–1537
37. Adzic RR, Wang JX (1998) Configuration and site of O_2 adsorption on the Pt(111) electrode surface. J Phys Chem B 102(45):8988–8993
38. Damjanovic A, Brusic V (1967) Electrode kinetics of oxygen reduction on oxide-free platinum electrodes. Electrochim Acta 12(6):615–628
39. Yeager E, Razaq M, Gervasio D, Razaq A, Tryk D (1992) The electrolyte factor in O_2 reduction electrocatalysis. In: Scheerson D, Tryk D, Daroux M, Xing X (eds) Structural effects in electrocatalysis and oxygen electrochemistry. Proc vol 92–11. The Electrochemical Society, Pennington NJ, p 440
40. Shao MH, Liu P, Adzic RR (2006) Superoxide anion is the intermediate in the oxygen reduction reaction on platinum electrodes. J Am Chem Soc 128(23):7408–7409
41. Griffith JS (1956) On the magnetic properties of some haemoglobin complexes. Proc R Soc Lond A 235(1200):23–36
42. Yeager E (1981) Recent advances in the science of the electrocatalysis. J Electrochem Soc 128(4):160C–171C
43. Marcus RA (1997) Electron transfer reactions in chemistry. Theory and experiment. J Electroanal Chem 438(1–2):251–259
44. Anderson AB, Albu TV (2000) Catalytic effect of platinum on oxygen reduction: an ab initio model including electrode potential dependence. J Electrochem Soc 147(11):4229–4238
45. Sidik RA, Anderson AB (2002) Density functional theory study of O_2 electroreduction when bonded to a Pt dual site. J Electroanal Chem 528(1–2):69–76
46. Li T, Balbuena PB (2003) Oxygen reduction on a platinum cluster. Chem Phys Lett 367(3–4): 439–447
47. Jinnouchi R, Okazaki K (2003) New insight into microscale transport phenomena in PEFC by quantum MD. Microscale Thermophys Eng 7(1):15–31
48. Hyman MP, Medlin JW (2007) Effects of electronic structure modifications on the adsorption of oxygen reduction reaction intermediates on model Pt(111)-alloy surfaces. J Phys Chem C 111(45):17052–17060
49. Li T, Balbuena PB (2001) Computational studies of the interactions of oxygen with platinum clusters. J Phys Chem B 105(41):9943–9952

50. Wang Y, Balbuena PB (2005) Potential energy surface profile of the oxygen reduction reaction on a Pt cluster: adsorption and decomposition of OOH and H_2O_2. J Chem Theory Comput 1(5):935–943
51. Valden M, Lai X, Goodman DW (1998) Onset of catalytic activity of gold clusters on titania with the appearance of nonmetallic properties. Science 281(5383):1647–1650
52. Meier J, Friedrich KA, Stimming U (2002) Novel method for the investigation of single nanoparticle reactivity. Faraday Discuss 121:365–372
53. Lopez N, Nørskov JK (2002) Catalytic CO oxidation by a gold nanoparticle: a density functional study. J Am Chem Soc 124(38):11262–11263
54. Maillard F, Eikerling M, Cherstiouk OV, Schreier S, Savinova E, Stimming U (2004) Size effects on reactivity of Pt nanoparticles in CO monolayer oxidation: the role of surface mobility. Faraday Discuss 125:357–377
55. Han BC, Miranda CR, Ceder G (2008) Effect of particle size and surface structure on adsorption of O and OH on platinum nanoparticles: a first-principles study. Phys Rev B 77(7):075410
56. Han BC, Ceder G (2006) Effect of coadsorption and Ru alloying on the adsorption of CO on Pt. Phys Rev B 74(20):205418
57. Xu Y, Ruban AV, Mavrikakis M (2004) Adsorption and dissociation of O_2 on Pt–Co and Pt–Fe alloys. J Am Chem Soc 126(14):4717–4725
58. Starke U, Materer N, Barbieri A, Döll R, Heinz K, Van Hove MA, Somorjai GA (1993) A low-energy-electron diffraction study of oxygen, water and ice adsorption on Pt(111). Surf Sci 287–288:432–437
59. Gland JL, Sexton BA, Fisher GB (1980) Oxygen interactions with the Pt(111) surface. Surf Sci 95(2–3):587–602
60. Watanabe M, Saegusa S, Stonehart P (1988) Electro-catalytic activity on supported platinum crystallites for oxygen reduction in sulphuric acid. Chem Lett 17(9):1487–1490
61. Giordano N, Passalacqua E, Pino L, Arico AS, Antonucci V, Vivaldi M, Kinoshita K (1991) Analysis of platinum particle size and oxygen reduction in phosphoric acid. Electrochim Acta 36(13):1979–1984
62. Takasu Y, Ohashi N, Zhang XG, Murakami Y, Minagawa H, Sato S, Yahikozawa K (1996) Size effects of platinum particles on the electroreduction of oxygen. Electrochim Acta 41(16): 2595–2600
63. Yano H, Inukai J, Uchida H, Watanabe M, Babu PK, Kobayashi T, Chung JH, Oldfield E, Wieckowski A (2006) Particle-size effect of nanoscale platinum catalysts in oxygen reduction reaction: an electrochemical and ^{195}Pt EC-NMR study. Phys Chem Chem Phys 8(42): 4932–4939
64. Mayrhofer KJJ, Blizanac BB, Arenz M, Stamenkovic VR, Ross PN, Markovic NM (2005) The impact of geometric and surface electronic properties of Pt-catalysts on the particle size effect in electrocatalysis. J Phys Chem B 109(30):14433–14440
65. Li X, Chen G, Xie J, Zhang L, Xia D, Wu Z (2010) An electrocatalyst for methanol oxidation in DMFC: PtBi/XC-72 with Pt solid-solution structure. J Electrochem Soc 157(4): B580–B584
66. Aricoo AS, Bruce P, Scrosati B, Tarascon JM, van Schalkwijk W (2005) Nanostructured materials for advanced energy conversion and storage devices. Nat Mater 4(5):366–377
67. Bing Y, Liu H, Zhang L, Ghosh D, Zhang J (2010) Nanostructured Pt-alloy electrocatalysts for PEM fuel cell oxygen reduction reaction. Chem Soc Rev 39(6):2184–2202
68. Antolini E (2003) Formation, microstructural characteristics and stability of carbon supported platinum catalysts for low temperature fuel cells. J Mater Sci 38(14):2995–3005
69. Stamenkovic VR, Fowler B, Mun BS, Wang G, Ross PN, Lucas CA, Markovic NM (2007) Improved oxygen reduction activity on $Pt_3Ni(111)$ via increased surface site availability. Science 315(5811):493–497

70. Stamenkovic V, Schmidt TJ, Ross PN, Markovic NM (2002) Surface composition effects in electrocatalysis: kinetics of oxygen reduction on well-defined Pt_3Ni and Pt_3Co alloy surfaces. J Phys Chem B 106(46):11970–11979
71. Zhang J, Mo Y, Vukmirovic MB, Klie R, Sasaki K, Adzic RR (2004) Platinum monolayer electrocatalysts for O_2 reduction: Pt monolayer on Pd(111) and on carbon-supported Pd nanoparticles. J Phys Chem B 108(30):10955–10964
72. Koh S, Strasser P (2007) Electrocatalysis on bimetallic surfaces: modifying catalytic reactivity for oxygen reduction by voltammetric surface dealloying. J Am Chem Soc 129(42): 12624–12625
73. Srivastava R, Mani P, Hahn N, Strasser P (2007) Efficient oxygen reduction fuel cell electrocatalysis on voltammetrically dealloyed Pt–Cu–Co nanoparticles. Angew Chem Int Ed 46(47):8988–8991
74. Mukerjee S, Srinivasan S, Soriaga MP, McBreen J (1995) Effect of preparation conditions of Pt alloys on their electronic, structural, and electrocatalytic activities for oxygen reduction-XRD, XAS, and electrochemical studies. J Phys Chem 99(13):4577–4589
75. Arico AS, Shukla AK, Kim H, Park S, Min M, Antonucci V (2001) An XPS study on oxidation states of Pt and its alloys with Co and Cr and its relevance to electroreduction of oxygen. Appl Surf Sci 172(1–2):33–40
76. Paulus UA, Wokaun A, Scherer GG, Schmidt TJ, Stamenkovic V, Radmilovic V, Markovic NM, Ross PN (2002) Oxygen reduction on carbon-supported Pt-Ni and Pt-Co alloy catalysts. J Phys Chem B 106(16):4181–4191
77. Markovic NM, Schmidt TJ, Stamenkovic V, Ross PN (2001) Oxygen reduction reaction on Pt and Pt bimetallic surfaces: a selective review. Fuel Cell 1(2):105–116
78. Drillet JF, Ee A, Friedemann J, Kotz R, Schnyder B, Schmidt V (2002) Oxygen reduction at Pt and $Pt_{70}Ni_{30}$ in H_2SO_4/CH_3OH solution. Electrochim Acta 47(12):1983–1988
79. Mukerjee S, Srinivasan S, Soriaga MP, McBreen J (1995) Role of structural and electronic properties of Pt and Pt alloys on electrocatalysis of oxygen reduction: an in situ XANES and EXAFS investigation. J Electrochem Soc 142(5):1409–1422
80. Min M, Cho J, Cho K, Kim H (2000) Particle size and alloying effects of Pt-based alloy catalysts for fuel cell applications. Electrochim Acta 45(25–26):4211–4217
81. Neergat M, Shukla AK, Gandhi KS (2001) Platinum-based alloys as oxygen-reduction catalysts for solid-polymer-electrolyte direct methanol fuel cells. J Appl Electrochem 31(4):373–378
82. Paffett MT, Barry JG, Gottesfeld S (1988) Oxygen reduction at $Pt_{0.65}Cr_{0.35}$, $Pt_{0.2}Cr_{0.8}$ and roughened platinum. J Electrochem Soc 135(6):1431–1436
83. Antolini E, Passos RR, Ticianelli EA (2002) Electrocatalysis of oxygen reduction on a carbon supported platinum–vanadium alloy in polymer electrolyte fuel cells. Electrochim Acta 48(3):263–270
84. Lai FJ, Chou HL, Sarma LS, Wang DY, Lin YC, Lee JF, Hwang BJ, Chen CC (2010) Tunable properties of Pt_xFe_{1-x} electrocatalysts and their catalytic activity towards the oxygen reduction reaction. Nanoscale 2(4):573–581
85. Toda T, Igarashi H, Uchida H, Watanabe M (1999) Enhancement of the electroreduction of oxygen on Pt alloys with Fe, Ni, and Co. J Electrochem Soc 146(10):3750–3756
86. Mukerjee S, Srinivasan S (1993) Enhanced electrocatalysis of oxygen reduction on platinum alloys in proton exchange membrane fuel cells. J Electroanal Chem 357(1–2):201–224
87. Antolini E, Salgado JRC, Gonzalez ER (2006) The stability of Pt–M (M = first row transition metal) alloy catalysts and its effect on the activity in low temperature fuel cells: a literature review and tests on a Pt–Co catalyst. J Power Sources 160(2):957–968
88. Colon-Mercado HR, Popov BN (2006) Stability of platinum based alloy cathode catalysts in PEM fuel cells. J Power Sources 155(2):253–263
89. Duan Z, Wang G (2011) A first principles study of oxygen reduction reaction on a Pt(111) surface modified by a subsurface transition metal M (M = Ni, Co, or Fe). Phys Chem Chem Phys 13(45):20178–20187

90. Nilekar AU, Mavrikakis M (2008) Improved oxygen reduction reactivity of platinum monolayers on transition metal surfaces. Surf Sci 602(14):L89–L94
91. Shao MH, Sasaki K, Adzic RR (2006) Pd−Fe nanoparticles as electrocatalysts for oxygen reduction. J Am Chem Soc 128(11):3526–3527
92. Fernandez JL, Raghuveer V, Manthiram A, Bard AJ (2005) Pd–Ti and Pd–Co–Au electrocatalysts as a replacement for platinum for oxygen reduction in proton exchange membrane fuel cells. J Am Chem Soc 127(38):13100–13101
93. Fernandez JL, Walsh DA, Bard AJ (2005) Thermodynamic guidelines for the design of bimetallic catalysts for oxygen electroreduction and rapid screening by scanning electrochemical microscopy. M–Co (M: Pd, Ag, Au). J Am Chem Soc 127(1):357–365
94. Savadogo O, Lee K, Oishi K, Mitsushimas S, Kamiya N, Ota KI (2004) New palladium alloys catalyst for the oxygen reduction reaction in an acid medium. Electrochem Commun 6(2):105–109
95. Savadogo O, Lee K, Mitsushima S, Kamiya N, Ota KI (2004) Investigation of some new palladium alloys catalysts for the oxygen reduction reaction in an acid medium. J New Mater Electrochem Syst 7(2):77–83
96. Raghuveer V, Manthiram A, Bard AJ (2005) Pd–Co–Mo electrocatalyst for the oxygen reduction reaction in proton exchange membrane fuel cells. J Phys Chem B 109(48): 22909–22912
97. Tarasevich MR, Zhutaeva GV, Bogdanovskaya VA, Radina MV, Ehrenburg MR, Chalykh AE (2007) Oxygen kinetics and mechanism at electrocatalysts on the base of palladium–iron system. Electrochim Acta 52(15):5108–5118
98. Opalka SM, Huang W, Wang D, Flanagan TB, Lovvik OM, Emerson SC, She Y, Vanderspurt TH (2007) Hydrogen interactions with the PdCu ordered B2 alloy. J Alloys Compd 446–447:583–587
99. Bittins-Cattaneo B, Wasmus S, Lopez-Mishima B, Vielstich W (1993) Reduction of oxygen in an acidic methanol/oxygen (air) fuel cell: an online MS study. J Appl Electrochem 23(6): 625–630
100. Gurau B, Smotkin ES (2003) Methanol crossover in direct methanol fuel cells: a link between power and energy density. J Power Sources 112(2):339–352
101. Shao MH, Huang T, Liu P, Zhang J, Sasaki K, Vukmirovic MB, Adzic RR (2006) Palladium monolayer and palladium alloy electrocatalysts for oxygen reduction. Langmuir 22(25): 10409–10415
102. Erikat IA, Hamad BA, Khalifeh JM (2011) A density functional study on adsorption and dissociation of O_2 on Ir(100) surface. Chem Phys 385(1–3):35–40
103. Zhang R, Liu H, Wang B, Ren J, Li Z (2011) Adsorption and dissociation of O_2 on CuCl(111) surface: a density functional theory study. Appl Surf Sci 258(1):408–413
104. Gasteiger HA, Kocha SS, Sompalli B, Wagner FT (2005) Activity benchmarks and requirements for Pt, Pt-alloy, and non-Pt oxygen reduction catalysts for PEMFCs. Appl Catal B 56(1–2):9–35
105. Chen Z, Higgins D, Yu A, Zhang L, Zhang J (2011) A review on non-precious metal electrocatalysts for PEM fuel cells. Energy Environ Sci 4(9):3167–3192
106. Bezerra CWB, Zhang L, Lee KC, Liu HS, Marques ALB, Marques EP, Wang HJ, Zhang JJ (2008) A review of Fe–N/C and Co–N/C catalysts for the oxygen reduction reaction. Electrochim Acta 53(15):4937–4951
107. van Veen J, Visser C (1979) Oxygen reduction on monomeric transition-metal phthalocyanines in acid electrolyte. Electrochim Acta 24(9):921–928
108. Wiesener K, Ohms D, Neumann V, Franke R (1989) N_4 macrocycles as electrocatalysts for the cathodic reduction of oxygen. Mater Chem Phys 22(3–4):457–475
109. Baranton S, Coutanceau C, Garnier E, Leger JM (2006) How does alpha-FePc catalysts dispersed onto high specific surface carbon support work towards oxygen reduction reaction (orr)? J Electroanal Chem 590(1):100–110

110. Baranton S, Coutanceau C, Roux C, Hahn F, Leger JM (2005) Oxygen reduction reaction in acid medium at iron phthalocyanine dispersed on high surface area carbon substrate: tolerance to methanol, stability and kinetics. J Electroanal Chem 577(2):223–234
111. Shi CN, Anson FC (1990) Catalytic pathways for the electroreduction of oxygen by iron tetrakis(4-N-methylpyridyl)porphyrin or iron tetraphenylporphyrin adsorbed on edge plane pyrolytic graphite electrodes. Inorg Chem 29(21):4298–4305
112. Cardenas-Jiron GI (2002) Substituent effect in the chemical reactivity and selectivity of substituted cobalt phthalocyanines. J Phys Chem A 106(13):3202–3206
113. Song EH, Shi CN, Anson FC (1998) Comparison of the behavior of several cobalt porphyrins as electrocatalysts for the reduction of O_2 at graphite electrodes. Langmuir 14(15):4315–4321
114. Vasudevan P, Mann SN, Tyagi S (1990) Transition metal complexes of porphyrins and phthalocyanines as electrocatalysts for dioxygen reduction. Transit Met Chem 15(2):81–90
115. Zhang L, Song CJ, Zhang JJ, Wang HJ, Wilkinson DP (2005) Temperature and pH dependence of oxygen reduction catalyzed by iron fluoroporphyrin adsorbed on a graphite electrode. J Electrochem Soc 152(12):A2421–A2426
116. Kadish KM, Fremond L, Ou ZP, Shao JG, Shi CN, Anson FC, Burdet F, Gros CP, Barbe JM, Guilard R (2005) Cobalt(III) corroles as electrocatalysts for the reduction of dioxygen: reactivity of a monocorrole, biscorroles, and porphyrin-corrole dyads. J Am Chem Soc 127(15): 5625–5631
117. Kobayashi N, Janda P, Lever ABP (1992) Cathodic reduction of oxygen and hydrogen peroxide at cobalt and iron crowned phthalocyanines adsorbed on highly oriented pyrolytic graphite electrodes. Inorg Chem 31(25):5172–5177
118. Shi C, Steiger B, Yuasa M, Anson FC (1997) Electroreduction of O_2 to H_2O at unusually positive potentials catalyzed by the simplest of the cobalt porphyrins. Inorg Chem 36(20): 4294–4295
119. Song C, Zhang L, Zhang J, Wilkinson DP, Baker R (2007) Temperature dependence of oxygen reduction catalyzed by cobalt fluoro-phthalocyanine adsorbed on a graphite electrode. Fuel Cells 7(1):9–15
120. Steiger B, Anson FC (1997) [5,10,15,20-tetrakis(4-((pentaammineruthenio)-cyano)phenyl) porphyrinato] cobalt(II) immobilized on graphite electrodes catalyzes the electroreduction of O_2 to H2O, but the corresponding 4-cyano-2,6-dimethylphenyl derivative catalyzes the reduction only to H_2O_2. Inorg Chem 36(18):4138–4140
121. Baker R, Wilkinson DP, Zhang JJ (2008) Electrocatalytic activity and stability of substituted iron phthalocyanines towards oxygen reduction evaluated at different temperatures. Electrochim Acta 53(23):6906–6919
122. Liu HS, Zhang L, Zhang JJ, Ghosh D, Jung J, Downing BW, Whittemore E (2006) Electrocatalytic reduction of O_2 and H_2O_2 by adsorbed cobalt tetramethoxyphenyl porphyrin and its application for fuel cell cathodes. J Power Sources 161(2):743–752
123. Wu G, Chen Z, Artyushkova K, Garzon FH, Zelenay P (2008) Polyaniline-derived non-precious catalyst for the polymer electrolyte fuel cell cathode. ECS Trans 16(2):159–170
124. Wu G, Artyushkova K, Ferrandon M, Kropf AJ, Myers D, Zelenay P (2009) Performance durability of polyaniline-derived non-precious cathode catalysts. ECS Trans 25(1): 1299–1311
125. Wu G, More KL, Johnston CM, Zelenay P (2011) High-performance electrocatalysts for oxygen reduction derived from polyaniline, iron, and cobalt. Science 332(6028):443–447
126. Sulub R, Martinez-Millan W, Smit MA (2009) Study of the catalytic activity for oxygen reduction of polythiophene modified with cobalt or nickel. Int J Electrochem Sci 4(7): 1015–1027
127. Khomenko VG, Barsukov VZ, Katashinskii AS (2005) The catalytic activity of conducting polymers toward oxygen reduction. Electrochim Acta 50(7–8):1675–1683
128. Martinez-Millan W, Smit MA (2009) Study of electrocatalysts for oxygen reduction based on electroconducting polymer and nickel. J Appl Polym Sci 112(5):2959–2967

129. Qin HY, Liu ZX, Yin WX, Zhu JK, Li ZP (2008) A cobalt polypyrrole composite catalyzed cathode for the direct borohydride fuel cell. J Power Sources 185(2):909–912
130. Chen J, Zhang WM, Officer D, Swiegers GF, Wallace GG (2007) A readily-prepared, convergent, oxygen reduction electrocatalyst. Chem Commun 32:3353–3355
131. Cong HN, El Abbassi K, Gautier JL, Chartier P (2005) Oxygen reduction on oxide/polypyrrole composite electrodes: effect of doping anions. Electrochim Acta 50(6): 1369–1376
132. Coutanceau C, Elhourch A, Crouigneau P, Leger JM, Lamy C (1995) Conducting polymer electrodes modified by metal tetrasulfonated phthalocyanines: preparation and electrocatalytic behaviour towards dioxygen reduction in acid medium. Electrochim Acta 40(17):2739–2748
133. Hirayama T, Manako T, Imai H (2008) A metal coordination polymer for fuel cell applications: nanostructure control toward high performance electrocatalysis. e J Surf Sci Nanotechnol 6:237–240
134. Reddy ALM, Rajalakshmi N, Ramaprabhu S (2008) Cobalt-polypyrrole-multiwalled carbon nanotube catalysts for H_2 and alcohol fuel cells. Carbon 46(1):2–11
135. Shao Y, Cong HN (2007) Oxygen reduction on high-area carbon cloth-supported oxide nanoparticles/polypyrrole composite electrodes. Solid State Ionics 178(23–24):1385–1389
136. Zhang WM, Chen J, Wagner P, Swiegers GF, Wallace GG (2008) Polypyrrole/Co-tetraphenylporphyrin modified carbon fibre paper as a fuel cell electrocatalyst of oxygen reduction. Electrochem Commun 10(4):519–522
137. Zhou Q, Li CM, Li J, Lu JT (2008) Electrocatalysis of template-electrosynthesized cobalt−porphyrin/polyaniline nanocomposite for oxygen reduction. J Phys Chem C 112(47): 18578–18583
138. Lee K, Zhang L, Lui H, Hui R, Shi Z, Zhang JJ (2009) Oxygen reduction reaction (ORR) catalyzed by carbon-supported cobalt polypyrrole (Co–PPy/C) electrocatalysts. Electrochim Acta 54(20):4704–4711
139. Yuan XX, Zeng X, Zhang HJ, Ma ZF, Wang CY (2010) Improved performance of proton exchange membrane fuel cells with p-toluenesulfonic acid-doped Co–PPy/C as cathode electrocatalyst. J Am Chem Soc 132(6):1754–1755
140. Yuasa M, Yamaguchi A, Itsuki H, Tanaka K, Yamamoto M, Oyaizu K (2005) Modifying carbon particles with polypyrrole for adsorption of cobalt ions as electrocatatytic site for oxygen reduction. Chem Mater 17(17):4278–4281
141. Alonso-Vante N, Tributsch H, Solorza-Feria O (1995) Kinetics studies of oxygen reduction in acid medium on novel semiconducting transition metal chalcogenides. Electrochim Acta 40(5):567–576
142. Cao DX, Wieckowski A, Inukai J, Alonso-Vante N (2006) Oxygen reduction reaction on ruthenium and rhodium nanoparticles modified with selenium and sulfur. J Electrochem Soc 153(5):A869–A874
143. Delacote C, Bonakdarpour A, Johnston CM, Zelenay P, Wieckowski A (2009) Aqueous-based synthesis of ruthenium–selenium catalyst for oxygen reduction reaction. Faraday Discuss 140:269–281
144. Fischer C, Alonsovante N, Fiechter S, Tributsch H (1995) Electrocatalytic properties of mixed transition metal tellurides (Chevrel-phases) for oxygen reduction. J Appl Electrochem 25(11):1004–1008
145. Lee K, Zhang L, Zhang JJ (2007) A novel methanol-tolerant Ir-Se chalcogenide electrocatalyst for oxygen reduction. J Power Sources 165(1):108–113
146. Lewera A, Inukai J, Zhou WP, Cao D, Duong HT, Alonso-Vante N, Wieckowski A (2007) Chalcogenide oxygen reduction reaction catalysis: X-ray photoelectron spectroscopy with Ru, Ru/Se and Ru/S samples emersed from aqueous media. Electrochim Acta 52(18): 5759–5765
147. Alonso-Vante N, Jaegermann W, Tributsch H, Honle W, Yvon K (1987) Electrocatalysis of oxygen reduction by chalcogenides containing mixed transition metal clusters. J Am Chem Soc 109(11):3251–3257

148. Alonso-Vante N, Tributsch H (1986) Energy conversion catalysis using semiconducting transition metal cluster compounds. Nature 323(6087):431–432
149. Doi S, Ishihara A, Mitsushima S, Kamiya N, Ota KI (2007) Zirconium-based compounds for cathode of polymer electrolyte fuel cell. J Electrochem Soc 154(3):B362–B369
150. Ishihara A, Lee K, Doi S, Mitsushima S, Kamiya N, Hara M, Domen K, Fukuda K, Ota K (2005) Tantalum oxynitride for a novel cathode of PEFC. Electrochem Solid State Lett 8(4): A201–A203
151. Liu Y, Ishihara A, Mitsushima S, Kamiya N, Ota K (2005) Zirconium oxide for PEFCs cathode. Electrochem Solid State Lett 8(8):A400–A402
152. Armstrong RD, Douglas AF, Williams DE (1971) A study of the sodium tungsten bronzes for use as electrocatalysts in acid electrolyte fuel cells. Energy Convers 11(1):7–10
153. Bockris JO, Mchardy J (1973) Electrocatalysis of oxygen reduction by sodium tungsten bronze: II. The influence of traces of platinum. J Electrochem Soc 120(1):61–66
154. Mchardy J, Bockris JO (1973) Electrocatalysis of oxygen reduction by sodium tungsten bronze: I. Surface characteristics of a bronze electrode. J Electrochem Soc 120(1):53–60
155. Houston JE, Laramore GE, Park RL (1974) Surface electronic properties of tungsten, tungsten carbide, and platinum. Science 185(4147):258–260
156. Levy RB, Boudart M (1973) Platinum-like behavior of tungsten carbide in surface catalyst. Science 181(4099):547–549
157. Binder H, Kohling A, Kuhn W, Lindner W, Sandsted G (1969) Tungsten carbide electrodes for fuel cells with acid electrolyte. Nature 224:1299–1300
158. Izhar S, Yoshida M, Nagai M (2009) Characterization and performances of cobalt–tungsten and molybdenum–tungsten carbides as anode catalyst for PEFC. Electrochim Acta 54(4): 1255–1262
159. Nikolov I, Vitanov T (1980) The effect of method of preparation on the corrosion resistance and catalytic activity during corrosion of tungsten carbide I. Corrosion resistance of tungsten carbide in sulfuric acid. J Power Sources 5(3):273–281
160. Palanker VS, Sokolsky DV, Mazulevsky EA, Baybatyrov EN (1976) Highly dispersed tungsten carbide for fuel cells with an acidic electrolyte. J Power Sources 1(2):169–176
161. Rees EJ, Essaki K, Brady CDA, Burstein GT (2009) Hydrogen electrocatalysts from microwave-synthesised nanoparticulate carbides. J Power Sources 188(1):75–81
162. Yang XG, Wang CY (2005) Nanostructured tungsten carbide catalysts for polymer electrolyte fuel cells. Appl Phys Lett 86(22):224104
163. Zhong HX, Zhang HM, Liu G, Liang YM, Hu JW, Yi BL (2006) A novel non-noble electrocatalyst for PEM fuel cell based on molybdenum nitride. Electrochem Commun 8(5): 707–712
164. Xia DG, Liu SZ, Wang ZY, Chen G, Zhang LJ, Zhang L, Hui SQ, Zhang JJ (2008) Methanol-tolerant MoN electrocatalyst synthesized through heat treatment of molybdenum tetraphenylporphyrin for four-electron oxygen reduction reaction. J Power Sources 177(2):296–302
165. Takagaki A, Takahashi Y, Yin FX, Takanabe K, Kubota J, Domen K (2009) Highly dispersed niobium catalyst on carbon black by polymerized complex method as PEFC cathode catalyst fuel cells and energy conversion. J Electrochem Soc 156(7):B811–B815
166. Yin FX, Takanabe K, Kubota J, Domen K (2010) Polymerized complex synthesis of niobium- and zirconium-based electrocatalysts for PEFC cathodes. J Electrochem Soc 157(2): B240–B244
167. Biddinger EJ, Deak D, Ozkan US (2009) Nitrogen-containing carbon nanostructures as oxygen-reduction catalysts. Top Catal 52(11):1566–1574
168. Gong K, Du F, Xia Z, Durstock M, Dai L (2009) Nitrogen-doped carbon nanotube arrays with high electrocatalytic activity for oxygen reduction. Science 323(5915):760–764
169. Kundu S, Nagaiah TC, Xia W, Wang Y, Dommele SV, Bitter JH, Santa M, Grundmeier G, Bron M, Schuhmann W, Muhler M (2009) Electrocatalytic activity and stability of nitrogen-containing carbon nanotubes in the oxygen reduction reaction. J Phys Chem C 113(32): 14302–14310

170. Lee KR, Lee KU, Lee JW, Ahn BT, Woo SI (2010) Electrochemical oxygen reduction on nitrogen doped graphene sheets in acid media. Electrochem Commun 12(8):1052–1055
171. Maldonado S, Stevenson KJ (2005) Influence of nitrogen doping on oxygen reduction electrocatalysis at carbon nanofiber electrodes. J Phys Chem B 109(10):4707–4716
172. Zhang L, Xia Z (2011) Mechanisms of oxygen reduction reaction on nitrogen-doped graphene for fuel cells. J Phys Chem C 115(22):11170–11176
173. Matter PH, Wang E, Arias M, Biddinger EJ, Ozkan US (2007) Oxygen reduction reaction activity and surface properties of nanostructured nitrogen-containing carbon. J Mol Catal A Chem 264(1–2):73–81
174. Qu L, Liu Y, Baek JB, Dai L (2010) Nitrogen-doped graphene as efficient metal-free electrocatalyst for oxygen reduction in fuel cells. ACS Nano 4(3):1321–1326
175. Imran Jafri R, Rajalakshmi N, Ramaprabhu S (2010) Nitrogen doped graphene nanoplatelets as catalyst support for oxygen reduction reaction in proton exchange membrane fuel cell. J Mater Chem 20(34):7114–7117
176. Titov A, Zapol P, Kral P, Liu DJ, Iddir H, Baishya K, Curtiss LA (2009) Catalytic Fe-*x*N sites in carbon nanotubes. J Phys Chem C 113(52):21629–21634
177. Kurak KA, Anderson AB (2009) Nitrogen-treated graphite and oxygen electroreduction on pyridinic edge sites. J Phys Chem C 113(16):6730–6734
178. Okamoto Y (2009) First-principles molecular dynamics simulation of O_2 reduction on nitrogen-doped carbon. Appl Surf Sci 256(1):335–341
179. Geng D, Chen Y, Chen Y, Li Y, Li R, Sun X, Ye S, Knights S (2011) High oxygen-reduction activity and durability of nitrogen-doped graphene. Energy Environ Sci 4(3):760–764
180. Chlistunoff J (2011) RRDE and voltammetric study of ORR on pyrolyzed Fe/polyaniline catalyst. On the origins of variable tafel slopes. J Phys Chem C 115(14):6496–6507
181. Ikeda T, Boero M, Huang SF, Terakura K, Oshima M, Ozaki J (2008) Carbon alloy catalysts: active sites for oxygen reduction reaction. J Phys Chem C 112(38):14706–14709
182. Matter PH, Zhang L, Ozkan US (2006) The role of nanostructure in nitrogen-containing carbon catalysts for the oxygen reduction reaction. J Catal 239(1):83–96
183. Maldonado S, Morin S, Stevenson KJ (2006) Structure, composition, and chemical reactivity of carbon nanotubes by selective nitrogen doping. Carbon 44(8):1429–1437
184. Subramanian NP, Li X, Nallathambi V, Kumaraguru SP, Colon-Mercado H, Wu G, Lee JW, Popov BN (2009) Nitrogen-modified carbon-based catalysts for oxygen reduction reaction in polymer electrolyte membrane fuel cells. J Power Sources 188(1):38–44
185. Rao CV, Cabrera CR, Ishikawa Y (2010) In search of the active site in nitrogen-doped carbon nanotube electrodes for the oxygen reduction reaction. J Phys Chem Lett 1(18):2622–2627
186. Wang XQ, Lee JS, Zhu Q, Liu J, Wang Y, Dai S (2010) Ammonia-treated ordered mesoporous carbons as catalytic materials for oxygen reduction reaction. Chem Mater 22(7):2178–2180
187. Jasinski R (1964) A new fuel cell cathode catalyst. Nature 201(4925):1212–1213
188. Sun S, Jiang N, Xia D (2011) Density functional theory study of the oxygen reduction reaction on metalloporphyrins and metallophthalocyanines. J Phys Chem C 115(19): 9511–9517
189. Shi Z, Zhang J (2007) Density functional theory study of transitional metal macrocyclic complexes' dioxygen-binding abilities and their catalytic activities toward oxygen reduction reaction. J Phys Chem C 111(19):7084–7090
190. Sun Y, Chen K, Jia L, Li H (2011) Toward understanding macrocycle specificity of iron on the dioxygen-binding ability: a theoretical study. Phys Chem Chem Phys 13(30): 13800–13808
191. Lu W, Fadeev AG, Qi B, Smela E, Mattes BR, Ding J, Spinks GM, Mazurkiewicz J, Zhou D, Wallace GG, Macfarlane DR, Forsyth SA, Forsyth M (2002) Use of ionic liquids for π-conjugated polymer electrochemical devices. Science 297(5583):983–987
192. Hepel M, Chen YM, Stephenson RJ (1996) Effect of the composition of polypyrrole substrate on the electrode position of copper and nickel. Electrochem Soc 143(2):498–505

193. Shi Z, Liu H, Lee K, Dy E, Chlistunoff J, Blair M, Zelenay P, Zhang J, Liu ZS (2011) Theoretical study of possible active site structures in cobalt–polypyrrole catalysts for oxygen reduction reaction. J Phys Chem C 115(33):16672–16680
194. Dipojono HK, Saputro AG, Aspera SM, Kasai H (2011) Density functional theory study on the interaction of O_2 molecule with cobalt–(6)pyrrole clusters. Jpn J Appl Phys 50(5):055702
195. Dipojono HK, Saputro AG, Belkada R, Nakanishi H, Kasai H, David M, Dy ES (2009) Adsorption of O_2 on cobalt–(*n*)pyrrole molecules. J Phys Soc Jpn 78(9):094710
196. Niwa H, Horiba K, Harada Y, Oshima M, Ikeda T, Terakura K, Ozaki J, Miyata S (2009) X-ray absorption analysis of nitrogen contribution to oxygen reduction reaction in carbon alloy cathode catalysts for polymer electrolyte fuel cells. J Power Sources 187(1):93–97
197. Biddinger EJ, Ozkan US (2010) Role of graphitic edge plane exposure in carbon nanostructures for oxygen reduction reaction. J Phys Chem C 114(36):15306–15314
198. Kim H, Lee K, Woo SI, Jung Y (2011) On the mechanism of enhanced oxygen reduction reaction in nitrogen-doped graphene nanoribbons. Phys Chem Chem Phys 13(39): 17505–17510
199. Calle-Vallejo F, Martínez JI, Rossmeisl J (2011) Density functional studies of functionalized graphitic materials with late transition metals for oxygen reduction reactions. Phys Chem Chem Phys 13(34):15639–15643
200. Yu L, Pan X, Cao X, Hu P, Bao X (2011) Oxygen reduction reaction mechanism on nitrogen-doped graphene: a density functional theory study. J Catal 282(1):183–190